Single-grain OSL dating of the Middle Palaeolithic site of Galería de las Estatuas, Atapuerca (Burgos, Spain)

Martina Demuro [1]*, Lee J. Arnold [1], Arantza Aranburu [2], Asier Gómez-Olivencia [3,4,5], Juan L. Arsuaga [5,6]

* corresponding author: martina.demuro@adelaide.edu.au

1 School of Physical Sciences, Environment Institute, and Institute for Photonics and Advanced Sensing (IPAS), University of Adelaide, North Terrace Campus, 5005 Adelaide, SA, Australia

2 Departamento Mineralogía y Petrología, Facultad de Ciencia y Tecnología, Universidad del País Vasco, Edificio F3, Barrio Sarriena s/n, 48940 Leioa, Bizkaia, Spain

3 Departamento de Estratigrafía y Paleontología, Facultad de Ciencia y Tecnología, Euskal Herriko Unibertsitatea, UPV-EHU, Barrio Sarriena s/n, 48940 Leioa, Spain

4 IKERBASQUE, Basque Foundation for Science, 48013 Bilbao, Spain

5 Centro Mixto Universidad Complutense-Instituto de Salud Carlos III de Evolución y Comportamiento Humanos, Avd. Monforte de Lemos 5, (Pabellón 14), 28029 Madrid, Spain

6 Departamento de Paleontología, Facultad de Ciencias Geológicas, Universidad Complutense de Madrid, c/ José Antonio Novais, Ciudad Universitaria, 28040 Madrid, Spain

Abstract

This study presents single-grain optically stimulated luminescence (OSL) chronologies for the archaeological site of Galería de las Estatuas – the first systematically excavated Middle Palaeolithic site within the karst system of the Sierra de Atapuerca archaeological complex, northern Spain. The single-grain OSL ages are compared with paired single-grain thermally transferred OSL (TT-OSL) dating results for a selection of samples in order to better assess quartz signal bleaching characteristics of endokarstic deposits preserved at Atapuerca. In total, seven luminescence dating samples were collected from four lithostratigraphic units exposed in two excavation pits (GE-I and GE-II). The single-grain OSL equivalent dose (D_e) distributions are characterised by generally low overdispersion (20-30%), suggesting appropriate bleaching at deposition. The resultant single-grain OSL ages reveal that the sediment sequence and archaeological remains excavated in pit GE-I accumulated 80-112 ka, while the upper layers of excavation area GE-II were deposited 70-79 ka. The replicate single-grain TT-OSL ages are in agreement with the OSL chronologies at 2σ for three of the four samples investigated; although in all cases the TT-OSL ages were systematically older than their single-grain counterparts. Apparent TT-OSL residual doses (i.e., TT-OSL D_e values in excess of their corresponding OSL D_e values) of 9 to 65 Gy were observed for all samples. These excess TT-OSL D_e values are generally low in comparison to the natural dose ranges of TT-OSL dating applications undertaken elsewhere in the Atapuerca karst system. The single-grain TT-OSL and OSL dating comparisons build on daylight bleaching experiments and modern analogue studies performed on other Atapuerca exogeneous

infill deposits and suggest reasonable potential for TT-OSL signal resetting down to relatively low levels for at least some sediments preserved in the Atapuerca karstic cavities. The quartz single-grain OSL chronologies obtained in this study place the Middle Palaeolithic sequence of Galería de las Estatuas within marine isotope stage (MIS) 5 and the beginning of MIS 4, and provide firm evidence for human occupation of the Sierra de Atapuerca during a previously unreported time period.

Keywords Single-grain OSL, TT-OSL, Atapuerca, Middle Palaeolithic, Neandertal, Iberia, Spain.

1. Introduction

The extensive karst system of the Sierra de Atapuerca (northern Iberian Plateau, Spain; **Figure 1a**) preserves several Early and Middle Pleistocene allochthonous infill sites (e.g., Gran Dolina, Galería complex, Sima del Elefante and Sima de los Huesos), which showcase important palaeoanthropological (*Homo antecessor* and early representatives of the Neandertal lineage; Bermúdez de Castro et al., 1997; Arsuaga et al., 2014), mammal faunal (Rodríguez et al., 2011) and Lower Palaeolithic records (Carbonell et al., 2008; Ollé et al., 2013), as well as extensive Upper Palaeolithic and Neolithic sequences (Carretero et al., 2008; Bañuls-Cardona et al., 2017). More than 30 Middle Palaeolithic open-air sites have additionally been discovered in the vicinity (<2 km) of the Atapuerca hills and surrounding river valleys (Navazo and Carbonell, 2014), and several of these sites have revealed rich Middle Palaeolithic assemblages (Navazo et al., 2011; Arnold et al., 2013). Until recently, however, equivalent Middle Palaeolithic records have not been reported from within the karst system (Aranburu et al., 2012). In this regard, Galería de las Estatuas represents an important new archaeological sequence within the Sierra de Atapuerca complex. It is the first Middle Palaeolithic site (<200 ka) to be systematically excavated within the endokarstic infill deposits of Atapuerca, and it is invaluable for providing improved insights into Neandertal occupational histories and subsistence/exploitation strategies in the region (Arsuaga et al., 2017).

The main archaeological and palaeoecological findings at Galería de las Estatuas have been summarised in Arsuaga et al. (2017) and include: (i) a lithic assemblage composed of 499 objects showing clear Mousterian affinities (e.g., centripetal flake cores, side-scrapers, denticulates), with some products displaying characteristic Levallois débitage; (ii) a detailed pollen record revealing, from the base upwards, a change from an open environment and dry/cool climate to a phase of shrub expansion, followed by an incremental increase in wooded species, and a more humid and warmer climate at the top of the sequence; and (iii) an extensive micro- and macro-mammal faunal record, with the latter being dominated by ungulates and displaying abundant evidence of human

modification (cut marks and anthropogenic breakage). The only chronological constraint available for this new site is a series of eight radiocarbon (^{14}C) ages obtained on faunal remains from levels LU1 and LU3, which range from 43.5 to >46.3 ^{14}C ka BP (uncalibrated), and a U-series age of ~14 ka obtained for the base of a stalagmitic crust capping the entire sedimentary sequence (Martínez-Pillado et al., 2014; Arsuaga et al., 2017). All of the ^{14}C ages are close to the analytical limits of the technique; five out of the eight samples yield infinite uncalibrated age ranges, and all eight samples yield non-finite 95.4% calibrated age ranges. Consequently, Arsuaga et al. (2017) cautiously interpreted these ^{14}C results as minimum ages and were only able to suggest that the archaeological accumulation at Galería de las Estatuas is likely of Late Pleistocene age. Given these problems, and the limited stratigraphic coverage of existing age control, there remains a need for a more comprehensive chronological study of the site.

The main aim of this study is to provide the first detailed chronological constraint on the various sediment layers at Galería de las Estatuas using single-grain optically stimulated luminescence (OSL) dating. We also present paired single-grain thermally transferred OSL (TT-OSL) dating comparisons for a subset of samples, with the aim of investigating the applicability of this approach for the Late Pleistocene infill karst deposits at Galería de las Estatuas. The majority of luminescence dating studies undertaken elsewhere on (>200 ka) sedimentary sequences at Atapuerca have used alternative 'extended-range' luminescence signals with higher dose saturation limits (Berger et al., 2008), including single-grain TT-OSL and post infrared IRSL dating (Demuro et al., 2014; Arnold et al., 2014; 2015; Arnold and Demuro, 2015). However, the relatively slow bleaching characteristics of TT-OSL signals (on the order of days, compared to seconds for the conventional OSL dating signal; Duller and Wintle, 2012; Duval et al., 2017) means that higher residual doses and age overestimation are a potential problem in this setting (Wang et al., 2006; Tsukamoto et al., 2008; Jacobs et al., 2011). An additional aim of this study is therefore to gain insights into TT-OSL signal resetting experienced by some of the younger Atapuerca karstic sediments, via assessments of quartz luminescence signals that bleach at different rates.

2. Site description and luminescence dating samples

The site of Galería de las Estatuas is situated 1020 masl in the uppermost level of the Cueva Mayor–Cueva del Silo karst system (**Figure S1**), adjacent to a palaeoentrance that has been sealed by a stalagmitic flowstone. Two test pits (<2 m-deep), denoted GE-I (9 m^2; ca. 2 m-deep) and GE-II (6 m^2; ca. 1.5 m-deep), have been excavated at this site. These test pits are located c. 18-20 m from the ancient cave entrance (Ortega, 2009). In GE-I, five lithostratigraphic units (LU) have been identified within the sedimentary sequence below the capping flowstone, while in GE-II, which has

been less extensively excavated, only two LUs have currently been identified (Arsuaga et al., 2017). Archaeological and palaeontological remains have been recovered from all LUs, although the material recovered from LU1 and LU5 in pit GE-I was relatively scarce. Sedimentological analyses of the LUs from both excavation pits indicate that the preserved sediment is allochthonous to the karst system (Aranburu et al., 2012; see Supplementary Information for further description of each LU). Transportation of these deposits into the cave interior is thought to have occurred via gravitational mass movement of water-saturated clays (i.e., debris flows), which simultaneously carried various proportions of clasts into the cavity (Arsuaga et al., 2017). The morphology of the gallery, as well as the position of the karstic infill deposits in relation to the cave entrance, suggest that the opening was a shallow ramp that allowed the progressive accumulation of fine-grain sediments and clasts under direct or indirect daylight, and ensured their subsequent transportation 20 m towards the cave interior during discrete runoff events (ramp inclination at the points of excavation is 5-8°). The allochthonous cave infill deposits being dated in this study originate from surface soils immediately surrounding the cave entrance, which contain a significant proportion of wind-blown silts and sands (Berger et al., 2008). Aeolian transportation and continued sub-aerial surface reworking of these sediments is likely to have favoured prolonged exposure to sunlight and full OSL signal resetting prior to being washed into the cave; as borne out by the very low residual D_e value obtained for modern surface sediments collected adjacent to several of the Atapuerca endokarst entrances (-0.03 ± 0.04 to 0.18 ± 0.07 Gy; see Arnold et al., in press). The relatively close proximity of the studied excavation pits to the original cave entrance is also thought to have favoured minimal sediment transportation residence times within the cavity prior to final deposition.

In total, seven luminescence dating samples were collected from the karstic infill deposits of Galería de las Estatuas as part of the present study: five samples were obtained from excavation pit GE-I (**Figure 1b**) and two samples were taken from pit GE-II (**Figure 1c**).

3. Luminescence dating methods

3.1 Instrumentation, dose rates and equivalent dose (D_e) estimation

Full details of the luminescence dating procedures employed in this study, including sample preparation, instrumentation, dose rate estimation, single-grain rejection criteria, and D_e measurement procedures, are provided in the Supplementary Information. Single-grain OSL dating was undertaken on all seven samples, while additional single-grain TT-OSL measurements were made on selected samples (GE16-1, GE16-4, GE16-6 and GE16-7). Environmental dose rates (**Table S1**) have been determined using a combination of in situ gamma spectrometry and low-level

beta counting. Cosmic-ray dose rates have been calculated using the approach described in Prescott and Hutton (1994).

Single-grain OSL and TT-OSL D_e measurements were made using the single-aliquot regenerative-dose (SAR) protocols described in Murray and Wintle (2000) and Stevens et al. (2009), respectively, which were modified to enable measurements of individual grains (e.g., Arnold et al., 2016; Demuro et al., 2014; **Table S3**). Single-grain dose recovery tests performed on both the OSL and TT-OSL signals support the suitability of the SAR protocols for dating these samples (corresponding dose recovery ratios = 0.98 ± 0.03 and 1.12 ± 0.14; see Supplementary Information, **Figure S2** and **Table S4**).

4. Results

4.1 Single-grain OSL signal characteristics and D_e estimates

Approximately 30-70% of the measured grains produced detectable OSL signals, with the brightest grains (1-3%) having 100-10,000 net counts / Gy in the first 0.09 s stimulation (**Figure 2a**). The measured OSL signals were also fast-decaying and were generally depleted by >90% within the first 0.18 s of stimulation. After applying the SAR rejection criteria, 4-9% of the measured grains were considered suitable for D_e estimation (**Table S5**). An example of a sensitivity-corrected dose-response and OSL decay curve for a moderately bright grain that passed the rejection criteria is shown in **Figure 2b**.

The single-grain OSL D_e distributions display relatively low scatter, with six out of the seven samples producing overdispersion values of 20-26% and one sample (GE16-7) producing a slightly higher, albeit consistent, overdispersion of 30 ± 4% (**Figure 3** and **Figure S4**; **Table 1**). None of the samples are considered to be significantly positively skewed according to the criterion outlined by Arnold and Roberts (2009). The overdispersion values of these karstic infill samples are also in agreement at 2σ with what is typically observed for well-bleached samples (~20%; Arnold and Roberts, 2009) and, with the exception of GE16-7, they are consistent at 2σ with the overdispersion value obtained in the dose-recovery test (10 ± 5%). Representative single-grain OSL burial dose estimates have therefore been calculated using the central age model (CAM) of Galbraith et al. (1999). The single-grain CAM D_e values obtained for the Galería de las Estatuas samples range between 85 to 145 Gy (**Table 1**).

The reliability of the single-grain OSL D_e estimates, as well as their usefulness for undertaking comparative TT-OSL bleaching assessments, will partly depend on whether the accepted grain

populations have sufficiently high dose saturation limits to ensure finite D_e estimation over the true natural burial dose ranges of interest (particularly as the measured D_e values typically exceed 100 Gy). To examine whether the single-grain OSL CAM D_e values have been compromised by dose saturation, we analysed the characteristic saturation dose (D_0) value for each accepted grain. The weighted mean (CAM) D_0 value for the combined Galería de las Estatuas sample dataset, calculated from all grains (n = 521), is 87 ± 1 Gy (**Figure S5**). The majority of accepted grains (~90%) produced D_0 values in the range of 40 to 160 Gy, with the remaining grains (~10%) having D_0 values of >160 Gy. In general, these D_0 values are high enough to enable finite D_e determination over the burial dose ranges of these samples (50-250 Gy); hence we do not consider that the single-grain OSL ages have been negatively affected by dose saturation. To explore this issue further, we applied the 2 × D_0 acceptance threshold criterion outlined by Demuro et al. (2015), which ensures that only grains with 2 × D_0 values higher than a specific burial dose are accepted for final D_e estimation. This additional quality assurance criterion is designed to eliminate grains that produce unrealistically low D_e values purely as a result of insufficient dose saturation limits, thus avoiding potential age underestimation arising from inherently unsuitable grains. Progressively higher 2 × D_0 thresholds of 140 to 260 Gy (increasing in 40 Gy increments) were applied to all the samples, and the effects on weighted mean D_e were examined after taking into consideration associated 2σ uncertainty ranges (see details in Arnold et al., 2016). For all seven samples, it was found that selecting grains with progressively higher D_0 values did not result in significantly higher CAM D_e values (**Figure S6**). Instead, both the CAM D_e and overdispersion (data not shown) remained within 2σ of the original values. Although a slight decrease in D_e is observed in samples GE16-4 and GE16-5 after a 2 × D_0 threshold of 220 Gy is applied, this trend is not deemed statistically significant since the resulting ages do not deviate beyond the 1σ ranges of the original values. These results indicate that the original single-grain OSL D_e values (and ages) calculated using all accepted grains were not adversely affected by OSL dose saturation.

4.2 Single-grain OSL ages

The single-grain OSL ages obtained for excavation pit GE-I are stratigraphically consistent and range between ~112 ka and ~80 ka (**Table 1**). These ages indicate that the sequence at GE-I was deposited during marine isotope stage (MIS) 5. The sedimentary sequence in excavation pit GE16-II (upper units) has a similar, albeit slightly younger, chronology, which extends from the end of MIS 5 to the beginning of MIS 4; stratigraphically consistent ages of 79 ± 5 ka (GE16-7) and 70 ± 5 ka (GE16-6) were obtained for LU2 and LU1, respectively. These single-grain OSL dating results suggest that the two sedimentary sequences excavated at Galería de las Estatuas potentially cover

the same time period (when considering their 2σ age ranges). The upper half of LU2 and LU1 in excavation pit GE-I are therefore likely correlative with LU2 from excavation pit GE-II.

4.3 Single-grain TT-OSL dating results

The majority of measured grains (60-80%) did not produce detectable TT-OSL signals (**Table S6**). Grains that did produce TT-OSL signals were generally very dim (e.g., the brightest 1% of grains produced 0.5-1 net counts / Gy / 0.09 s; **Figure 2a**), with only 1-5% of measured grains being accepted for final D_e estimation (**Table S6**). An example of a representative TT-OSL dose response and decay curve for an accepted grain is shown in **Figure 2c**. The single-grain TT-OSL D_e distributions of samples GE16-1, GE16-4 and GE16-7 were generally less scattered than their OSL counterparts (overdispersion values were 18-21%), with only sample GE16-6 having a higher overdispersion (45%) (**Table 1**; **Figure S7**). All four samples produced CAM D_e values that were higher (by 9 to 65 Gy) than their corresponding single-grain OSL CAM D_e values (after correcting for dose rate differences related to the different grain sizes being measured). However, three of the four samples (GE16-4, GE16-6 and GE16-7) produced final single-grain TT-OSL ages in agreement with their paired single-grain OSL ages at 2σ (**Table 1**).

The TT-OSL age of GE16-7 (84 ± 7 ka) was in closest agreement with its OSL counterpart (79 ± 5 ka), and this sample may be regarded as having experienced adequate TT-OSL signal bleaching at deposition. The low number of D_e values obtained for GE16-4 (n = 14; **Table 1**), and the large uncertainty associated with the final age estimate, potentially complicate the interpretations of TT-OSL bleaching adequacy for this sample. The TT-OSL and OSL ages of this sample are in agreement at 2σ but additional single-grain TT-OSL measurements would be needed to confirm its TT-OSL bleaching history. For sample GE16-6, the CAM TT-OSL age (86 ± 8 ka) is within 2σ of the OSL age (70 ± 5 ka) but the large overdispersion obtained for the TT-OSL dataset (45 ± 7%) (**Table 1**) may indicate additional, extrinsic D_e scatter related to minor populations of partially bleached grains (**Figure 3**). Application of the 3-parameter and 4-parameter minimum age models (MAM-3 and MAM-4; Galbraith et al., 1999) to this TT-OSL D_e dataset produced ages that were systematically younger than (though within 2σ of) the single-grain OSL age of GE16-6 (in italics **Table 1**). Sample GE16-1 displays the highest offset between its replicate single-grain TT-OSL and OSL ages. Although the TT-OSL D_e dataset for this sample has a low overdispersion of 20 ± 6%, which may indicate full signal resetting, the TT-OSL CAM D_e is ~50% higher than its OSL counterpart, and the resulting TT-OSL age (123 ± 10 ka) overestimates the OSL age (83 ± 5 ka) beyond its 2σ uncertainty ranges. It may be worth noting that the single-grain TT-OSL dose recovery test performed on this sample yielded a measured-to-given dose ratio that was

systematically in excess of unity by ~12% (albeit consistent with the given dose at 2σ). The higher TT-OSL age for sample GE16-1 may therefore partly originate from intrinsic D_e scatter related to the chosen SAR measurement protocol.

5. Discussion and conclusion

The single-grain TT-OSL and OSL dating comparisons undertaken in this study build on daylight bleaching experiments and modern analogue studies performed elsewhere on Atapuerca exogeneous infill deposits (Demuro et al., 2015, Arnold et al., in press), and suggest reasonable potential for TT-OSL signal resetting down to relatively low levels for some sediments preserved in the Atapuerca karstic cavities. All four samples contained large populations of grains with seemingly well-bleached TT-OSL signals, indicating prolonged (>6 weeks; Demuro et al., 2015, Arnold et al., in press) exposure to sunlight prior to burial within the cave. The single-grain TT-OSL ages are in agreement with the replicate OSL chronologies at 2σ for three of the four samples investigated; although in all cases the TT-OSL ages were systematically older than their single-grain counterparts. Mean TT-OSL residual doses (calculated as the difference between paired OSL and TT-OSL CAM D_e values) varied widely for the four samples, ranging between ~9 and ~65 Gy after correcting for grain-size dosimetric effects. These results suggest that it may be unsuitable to generalise about TT-OSL dating adequacy for allochthonous cave infill deposits without undertaking site-specific assessments. As our dating comparisons demonstrate, a useful approach for assessing TT-OSL bleaching adequacy involves simultaneously applying a suite of luminescence signals that are optically reset at different rates (i.e., OSL, pIR-IR), particularly when reliable independent age control is unavailable (e.g., Demuro et al., 2014; 2015; Hamm et al., 2016; Jacobs et al., 2017; Arnold et al., in press). In general, the mean TT-OSL residual doses observed at Galería de las Estatuas are relatively low in comparison to the natural dose ranges of TT-OSL dating applications undertaken elsewhere in the Atapuerca karst system (either due to their high environmental dose rates or older depositional ages). Residual D_e values on the order of several Gy or tens of Gy are likely to be well within the existing 2σ TT-OSL age uncertainties for most Middle or Early Pleistocene samples, and therefore are unlikely to have major effects on extended-range TT-OSL dating reliability.

Our single-grain OSL ages for Galería de las Estatuas place the sedimentary sequence of excavation pit GE-I (**Figure 4**) within MIS 5 (80 ± 5 ka to 112 ± 7 ka) and the sequence at excavation pit GE-II (upper section) within late MIS 5 and early MIS 4 (70 ± 5 ka to 79 ± 5 ka); though the chronologies of GE-I and GE-II are statistically indistinguishable at 2σ. As expected, these luminescence chronologies are older than the preliminary ^{14}C ages reported for the site (>45 cal ka BP – >49.5 cal

ka BP; **Table S7**), confirming the original interpretation of Arsuaga et al. (2017) that their ^{14}C results should be considered as minimum age estimates. Our ages for GE-I and GE-II are stratigraphically consistent and suggest that the two sequences excavated at Galería de las Estatuas are likely temporally correlative, although further dating at the base of pit GE-II is required to determine the lower chronological range of this sequence. It is worth noting that the age of sample GE16-3 (113 ± 8 ka), which was collected from a localised sub-layer at the base of LU2, is in closer agreement with the age obtained for the underlying level (LU3) (107 ± 8 ka; GE16-4), rather than the age obtained for the upper section of LU2 (83 ± 5 ka; GE16-1). Further dating efforts and more detailed sedimentological studies of this sub-layer may be necessary to ascertain its exact chronostratigraphic relationship with LU2 and LU3. Together, the single-grain OSL ages obtained for GE-I indicate that the pollen-based climatic reconstructions at this excavation pit – which show a change from an open environment and dry/cool conditions (lower LU3 and LU4) towards a phase of shrub expansion (upper LU3) and a more humid and warmer climate, followed by an increase in wooded species (LU2) at the top of the sequence – may be associated with MIS 5.4 (LU3-4) and MIS 5.1 (LU2), respectively (Lisiecki and Raymo, 2005; **Figure 4**). Although it is difficult to make more precise correlations between the climatic reconstructions at Galería de las Estatuas and global $\delta^{18}O$ isotope stages, both the pollen record and the chronologies obtained suggest that LU4 was deposited post-MIS 5.5 (**Figure 4**).

Galería de las Estatuas is the first archaeological site within the Sierra de Atapuerca karst system to be dated to MIS 4/5. Within a regional context, several other Middle Palaeolithic and Neandertal sites from the surrounding valleys of the northern Iberian meseta region could be considered to be chronologically equivalent to Galería de las Estatuas (**Table S7**). The open-air sequences of Hotel California and Hundidero, located in the vicinity of the Atapuerca hills, have chronologies of 70-45 ka based on single-grain OSL and TL dating of sedimentary grains, respectively (Arnold et al., 2013; Navazo et al., 2011), and may be partially correlative with, albeit slightly younger than, Galería de las Estatuas. The Neandertal cave site of Valdegoba located a short (<30 km) distance from Atapeurca may also have a similar chronology. The sequence is capped by a speleothem that has been U-series dated to <73.2 ± 5 ka (Quam et al., 2001). An additional AMS ^{14}C ultrafiltration age of 48.4 ± 3.3 ka (uncalibrated) has been obtained from the human-bearing layers of Valdegoba Dalén et al. (2008), which may be regarded as a minimum age due to its antiquity. La Ermita, another nearby cave site (Díez et al., 2008), could also be dated to MIS 5. This site has a ^{14}C age of 32.1–34.2 ka cal BP (Díez et al., 2008), but a U-series age of 95-102 ka has been recently reported for a speleothem capping the sediment sequence (Sánchez Yustos and Diez Martín, 2016). Other sites with similar chronologies on the Iberian plateau include San Quirce (73 ± 10 ka; Terradillos-

Bernal et al., 2017) and Cueva del Camino, near Madrid (74-140 ka; Arsuaga et al., 2012). While in the Cantabrian Range to the north, the site of El Castillo also covers a similar time span (level 23 ~90 ka; Bischoff et al., 1992). However, further dating studies are required at some of these sites to fully elucidate the Late Pleistocene Neandertal occupation histories in the region, especially in cases where ^{14}C dating appear to have reached its upper limits (**Table S7**). The chronological results obtained in the present study for Galería de las Estatuas indicate that single-grain OSL dating has the potential to make important contributions towards this effort.

Acknowledgements

We dedicate this paper to Glen Berger who worked closely with the excavation and research teams at Atapuerca over many years. Financial support for this research was provided by Australian Research Council (ARC) Discovery Early Career Researcher Award DE160100743 and Future Fellowship project FT130100195. We would like to acknowledge the entire GE excavation and research team, and especially the people that helped during sample collection. Fieldwork at Atapuerca was funded by the Junta de Castilla y León and Fundación Atapuerca. The study was supported by the Spanish Ministerio de Ciencia y Tecnología (Projects: CGL2012-38434-C03-01, CGL-2015-65387-C3-2-P) (MINECO/FEDER). AGO is part of Research Group IT1044-16 (Gobierno Vasco/Eusko Jaurlaritza) and is also funded by Research Group PPG17/05 (Euskal Herriko Unibertsitatea).

Figure captions

Figure 1. (A) Map of the Iberian Peninsula showing the location of the Galería de las Estatuas archaeological site (Atapuerca). (B) Photo of excavation pit GE-I showing the profile exposed on the western and northern faces and the position of the five samples collected for luminescence dating. (C) Photo of excavation pit GE-II showing the profile on the southern face and the position of the two luminescence dating samples collected.

Figure 2. (A) OSL signal brightness plot showing absolute net intensities expressed as counts / Gy / 0.09 s. The data shown are for single-grain OSL measurements made using the 212-250 μm quartz fraction for all samples except GE16-4, for which the 250-300 um fraction was used; also shown is the single-grain TT-OSL signal brightness plot for the 250-300 μm fraction of sample GE16-4 (1 grain per hole). Examples of (B) OSL and (C) TT-OSL decay curves and sensitivity-corrected dose-response curves (inset) for two grains from samples GE16-1 and GE16-6.

Figure 3. Radial plots showing the paired single-grain OSL and single-grain TT-OSL D_e distributions obtained for samples (A) GE16-1 and (B) GE16-6 (D_e errors are shown at 1σ). The grey band is centred on the central age model D_e obtained for the OSL dataset.

Figure 4. Single-grain OSL ages (and associated 1σ errors) for the seven luminescence samples collected from Galería de las Estatuas (black circles), plotted against and the $\delta^{18}O$ isotope curves for the last glacial cycle (NGRIP and Intermediate North Atlantic records). The ages obtained for each

excavation pit are shown on separate panels (GE-I in lower panel; GE-II in upper panel) because the lithostratigraphic unit (LU) numbering systems have been assigned independently for each excavated sequence (Arsuaga et al., 2017). Also shown are the single-grain TT-OSL ages obtained using the central age model (CAM) (white triangles). The continuous capping speleothem extends across both excavation pits, and its age (white circle) is based on previously published data (Martínez-Pillado et al., 2014). The grey hashed lines indicate tentative (spatially averaged) positions of the LU boundaries.

References

Andersen, K.K., Azuma, N., , Barnola, J.-M., Bigler, M., Biscaye, P., Caillon, N., Chappellaz, J., Clausen, H.B., Dahl-Jensen, D., Fischer, H., Flückiger, J., Fritzsche, D., Fujii, Y., Goto-Azuma, K., Grønvold, K., Gundestrup, N. S., Hansson, M., Huber, C., Hvidberg, C. S., Johnsen, S. J., Jonsell, U., Jouze, J., Kipfstuh, S., Landais, A., Leuenberger, M., Lorrain, R., Masson-Delmotte, V., Miller, H., Motoyama, H., Narita, H., Popp, T., Rasmussen, S.O., Raynaud, D., Rothlisberger, R., Ruth, U., Samyn, D., Schwander, J., Shoji, H., Siggard-Andersen, M.-L., Steffensen, J.P., Stocker, T., Sveinbjörnsdóttir, A.E., Svensson, A., Takata, M., Tison, J.-L., Thorsteinsson, Th., Watanabe, O., Wilhelms, F., White, J.W.C., 2004. High-resolution record of Northern hemisphere climate extending into the last interglacial period. Nature 431, 147-151.

Aranburu, A., Martínez-Pillado, V., Arsuaga, J.L., Alcázar de Velasco, A., et al., 2012. La variabilidad de los rellenos endokársticos de la Galería de Estatuas (Atapuerca, Burgos) y su caracterización paleoambiental. In: González-Díez, A., et al. (Eds.), Avances de la Geomorfología en España 2010-2012. Actas de la XII Reunión Nacional de Geomorfología. Santander, 17-20 September 2012.

Arnold L.J., Roberts, R.G., 2009. Stochastic modelling of multi-grain equivalent dose (D_e) distributions: Implications for OSL dating of sediment mixtures. Quaternary Geochronology 4, 204–230.

Arnold, L.J., Demuro, M., Navazo Ruiz, M., 2012. Empirical insights into multi-grain averaging effects from 'pseudo' single-grain OSL measurements. Radiation Measurements 47, 652-658.

Arnold, L.J., Demuro, M., Navazo Ruiz, M., Benito-Calvo, A., Pérez-González, A., 2013. OSL dating of the Middle Palaeolithic Hotel California site, Sierra de Atapuerca, north-central Spain. Boreas 42, 285-305.

Arnold, L.J., Demuro, M., Parés, J.M., Arsuaga, J.L., Aranburu, A., Bermúdez de Castro, J.M., Carbonell, E., 2014. Luminescence dating and palaeomagnetic age constraint on hominins from Sima de los Huesos, Atapuerca, Spain. Journal of Human Evolution 67, 85-107.

Arnold, L.J., Demuro, M., Parés, J.M., Pérez-González, A., Arsuaga, J.L., Bermúdez de Castro, J.M., Carbonell, E., 2015. Evaluating the suitability of extended-range luminescence dating techniques over Early and Middle Pleistocene timescales: Published datasets and case studies from Atapuerca, Spain. Quaternary International 389, 167-190.

Arnold, L.J., Demuro, M., 2015. Insights into TT-OSL signal stability from single-grain analyses of known-age deposits at Atapuerca, Spain. Quaternary Geochronology 30, 472-478.

Arnold, L.J., Duval, M., Demuro, M., Spooner, N.A., Santonja, M., Pérez-González, A., 2016. OSL dating of individual quartz 'supergrains' from the Ancient Middle Palaeolithic site of Cuesta de la Bajada, Spain. Quaternary Geochronology 36, 78-101.

Arnold, L.J., Demuro, M., Spooner, N.A., Prideaux, G.J., McDowell, M.C., Camens, A.B., Reed, E.H., Parés, J.M., Arsuaga, J.L., Bermúdez de Castro, J.M., Carbonell, E., Single-grain TT-OSL bleaching characteristics: insights from modern analogues and OSL dating comparisons. Quaternary Geochronology, in press, doi.org/10.1016/j.quageo.2018.01.004.

Arsuaga J.L., Baquedano, E., Pérez-González, A., Sala, N., Quam, R.M., Rodríguez, L., García, R., García, N., Alvarez-Lao, D.J., Laplana, C., Huguet, R., Sevilla, P., Maldonado, E., Blain, H-A., Ruiz-Zapata, M.B., Sala, P., Gil-García, J., Uzquiano, P., Pantoja, A., Márquez, B., 2012. Understanding the ancient habitats of the last interglacial (late MIS 5) Neanderthals of central Iberia: Paleoenvironmental and taphonomic evidence from the Cueva del Camino (Spain) site. Quaternary International 275, 55-75.

Arsuaga, J.L., Martínez, I., Arnold, L.J., Aranburu, A., Gracia-Téllez, A., Sharp, W.D., Quam, R.M., Falguères, C., Pantoja-Pérez, A., Bischoff, J., Poza-Rey, E., Parés, J.M., Carretero, J.M., Demuro, M., Lorenzo, C., Sala, N., Martinón-Torres, M., García, N., Alcázar de Velasco, A., Cuenca-Bescós, G., Gómez-Olivencia, A., Moreno, D., Pablos, A., Shen, C.-C., Rodríguez, L., Ortega, A.I., García, R., Bonmatí, A., Bermúdez de Castro, J.M., Carbonell, E., 2014. Neandertal roots: Cranial and chronological evidence from Sima de los Huesos. Science 344, 1358-1363.

Arsuaga, J.L., Gómez-Olivencia, A., Sala, N., Martínez-Pillado, V., Pablos, A., Bonmatí, A., Pantoja-Pérez, A., Lira-Garrido, J., Alcázar de Velasco, A., Ortega, A.I., Cuenca-Bescós, G., García, N., Aranburu, A., Ruiz-Zapata, B., Gil-García, M.J., Rodríguez-Alvarez, X.P., Ollé, A., Mosquera, M., 2017. Evidence of paleoecological changes and Mousterian occupations at the Galeria de las Estatuas site, Sierra de Atapuerca, norther Iberian plateau, Spain. Quaternary Research 88, 345-367.

Bañuls-Cardona, S., López-García, J.M., Morales Hidalgo, J.I., Cuenca-Bescós, G., Vergès, J.M., 2017. Lateglacial to Late Holocene palaeoclimatic and palaeoenvironmental reconstruction of El Mirador cave (Sierra de Atapuerca, Burgos, Spain) using the small-mammal assemblages. Palaeogeography, Palaeoclimatology, Palaeoecology 471, 71-81.

Berger, G.W., Pérez-González, A., Carbonell, E., Arsuaga, J.L., Bermúdez de Castro, J.-M., Ku, T.-L., 2008. Luminescence chronology of cave sediments at the Atapuerca paleoanthropological site, Spain. Journal of Human Evolution 55, 300–311.

Bermúdez de Castro, J.M., Arsuaga, J.L., Carbonell, E., Rosas, A., Martínez, I., Mosquera, M., 1997. A hominid from the Lower Pleistocene of Atapuerca, Spain: Possible ancestor to neandertals and modern humans. Science 276, 1392-1395.

Bischoff, J.L., Garcia, J.F., Straus, G., 1992. Uranium-series isochron dating at El Castillo cave (Cantabria, Spain): the "Acheulean"/"Mousterian" question. Journal of Archaeological Science 19, 49-92.

Carbonell, E., Bermúdez de Castro, J.M., Parés, J.M., Pérez-González, A., Ollé, A., Mosquera, M., Cuenca-Bescós, G., García, N., Granger, D.E., Huguet, R., van der Made, J., Martinón-Torres, M., Rodríguez, X.P., Rosas, A., Sala, R., Stock, G.M., Vallverdu, J., Vergés, J.M., Allué, E., Benito, A., Burjachs, F., Cáceres, I., Canals, A., Díez, J.C., Lozano, M., Mateos A., Navazo, M., Rodríguez, J., Rosell, J., Arsuaga, J.L., 2008. The first hominin of Europe. Nature 452, 465-469.

Carretero, J.M., Ortega, J.M., Juez, A.I., Pérez-González, A., Arsuaga, J.L., Pérez-Martínez, R., Ortega, M.C., 2008. A Late Pleistocene-Early Holocene archaeological sequence of Portalón de Cueva Mayor (Sierra de Atapuerca, Burgos, Spain). Munibe (Antropologia - Arkeologia) 59, 67-80.

Dalén, L., Orlando, L., Shapiro, B., Brandström-Durling, M., Quam, R., Thomas, M., Gilbert, P., Díez Fernández-Lomana, J.C., Willerslev, E., Arsuaga, J.L., Gotherström, A., 2012. Partial genetic turnover in Neanderthals: continuity in the east and population replacement in the west. Mol Biol Evol 29, 1893-1897.

Demuro, M., Arnold, L.J., Parés, J.M., Pérez-González, A., Ortega, A.I., Arsuaga, J.L., Bermúdez de Castro, J.M., Carbonell, E., 2014. New luminescence ages for the Galería Complex archaeological site: Resolving chronological uncertainties on the Acheulean record of the Sierra de Atapuerca, northern Spain. PLOS ONE 9, e110169.

Demuro, M., Arnold, L.J., Parés, J.M., Sala, R., 2015. Extended-range luminescence chronologies suggest potentially complex bone accumulation histories at the Early-to-Middle Pleistocene palaeontological site of Huéscar-1 (Guadix-Baza basin, Spain). Quaternary International 389, 191-212.

Díez, C., Alonso, R., Bengoechea, A., Colina, A., Jordá, J.F., Navazo, M., Ortiz, J.E., Pérez, S., Torres, T., 2008. El Paleolítico Medio en el valle del Arlanza (Burgos), los sitios de La Ermita, Millán y La Mina. Quaternario Geo-morfolgía 22, 135-157.

Duval, M., Arnold, L., V. Guilarte, M. Demuro, M. Santonja and A. Pérez-Gonzalez., 2017. Electron Spin Resonance dating of optically bleached quartz grains from the Middle Palaeolithic site of Cuesta de la Bajada (Spain) using the multiple centres approach. Quaternary Geochronology 37, 82-96.

Duller, G.A.T., Wintle, A.G., 2012. A review of the thermally transferred optically stimulated luminescence signal from quartz for dating sediments. Quaternary Geochronology 7, 6-20.

Galbraith, R.F., Roberts, R.G., Laslett, G.M., Yoshida, H., Olley, J.M., 1999. Optical dating of single and multiple grains of quartz from Jinmium rock shelter, northern Australia: Part I, experimental design and statistical models. Archaeometry 41, 339-364.

Hamm, G., Mitchell, P., Arnold, L.J., Prideaux, G.J., Questiaux, D., Spooner, N.A., Levchenko, V.A., Foley, E.C., Worthy, T.H., Stephenson, B., Coulthard, V., Coulthard, C., Wilton, S., Johnston, D., 2016. Cultural innovation and megafauna interaction in the early settlement of arid Australia. Nature 539, 280-283.

Jacobs, Z., Roberts, R.G., Lachlan, T.J., Karkanas, P., Marean, C.W., Roberts, D.L., 2011. Development of the SAR TT-OSL procedure for dating Middle Pleistocene dune and shallow marine deposits along the southern Cape coast of South Africa. Quaternary Geochronology 6, 491-513.

Jacobs, Z., Li, B., Farr, L., Hill, E., Hunt, C., Jones, S., Rabett, R., Reynolds, T., Roberts, R.G., Simpson, D., Barker, G., 2017. The chronostratigraphy of the Haua Fteah cave (Cyrenaica, northeast Libya) — Optical dating of early human occupation during Marine Isotope Stages 4, 5 and 6. Journal of Human Evolution 105, 69-88.

Lisiecki, L.E., Raymo, M.E., 2005. A Pliocene-Pleistocene stack of 57 globally distributed benthic δ18O records. Paleoceanography 20, PA 1003.

Lisiecki, L.E., Stern, J.V., 2016. Regional and global benthic $\delta^{18}O$ stacks for the last glacial cycle. Paleoceanography 31, 1364-1394.

Martínez-Pillado, V., Aranburu, A., Arsuaga, J.L., Ruiz-Zapata, B., Gil-García, M.J., Stoll, H., Yusta, I., Iriarte, E., Carretero, J.M., Edwards, R.L., Cheng, H., 2014. Upper Pleistocene and Holocene palaeoenvironmental records in Cueva Mayor karst (Atapuerca, Spain) from different proxies: speleothem crystal fabrics, palynology, and archaeology. International Journal of Speleology 43, 1-14.

Murray, A.S., Wintle, A., 2000. Luminescence dating of quartz using an improved single-aliquot regenerative-dose protocol. Radiation Measurements 32, 57–73.

Navazo, M., Carbonell, E., 2014. Neanderthal settlement patterns during MIS 4–3 in Sierra de Atapuerca (Burgos, Spain). Quaternary International 331, 267-277.

Navazo, M., Alonso-Alcalde, R., Benito-Calvo, A., Diez, J.C., Perez-Gonzalez, A., Carbonell, E., 2011. Hundidero: MIS 4 open air Neanderthal occupations in Sierra de Atapuerca. Archaeology Ethnology & Anthropology of Eurasia 39, 29-41.

Ollé, A., Mosquera, M., Rodríguez, X.P., Lombera-Hermida, A., García-Antón, M.D., García-Medrano, P., Peña, L., Menéndez, L. Navazo, M., Terradillos, M., Bargalló, A., Márquez, B., Sala, R., Carbonell, E., 2013. The Early Middle Pleistocene technological record from Sierra de Atapuerca (Burgos, Spain). Quaternary International 295, 138–167.

Ortega, A.I., 2009. Evolución geomorfológica del Karst de la Sierra de Atapuerca (Burgos) y su relación con los yacimientos pleistocenos que contiene. Ph.D. Dissertation. Universidad de Burgos.

Prescott, J.R., Hutton, J.T., 1994. Cosmic ray contributions to dose rates for luminescence and ESR dating: large depths and long-term time variations. Radiation Measurements 23, 497-500.

Quam, R.M., Arsuaga, J.L., Bermúdez de Castro, J.M., Díez, C.J., Lorenzo, C., Carretero, J.M., García, N., Ortega, A.I., 2001. Human remains from Valdegoba Cave (Huérmeces, Burgos, Spain). Journal of Human Evolution 41, 385-435.

Rodríguez, J., Burjachs, F., Cuenca-Bescós, G., García, N., Van der Made, J., Pérez-González, A., Blain, H.-A., Expósito, I., Lopez-García, J.M., García Antón, M., Allué, E., Cáceres, I., Huguet, R., Mosquera, M., Ollé, A., Rosell, J., Parés, J.M., Rodríguez, J.M., Díez, C., Rofes, J., Sala, R., Saladié, P., Vallverdú, J., Bennasar, M.L., Blasco, R., Bermúdez de Castro, J.M., Carbonell, E., 2011. One million years of cultural evolution in a stable environment at Atapuerca (Burgos, Spain). Quaternary Science Reviews 30, 1396–1412.

Sánchez Yustos, P., Diez Martín, F., 2016. Dancing to the rhythms of the Pleistocene? Early Middle Palaeolithic populations dynamics in NW Iberia (Duero Basin and Cantabrian Region). Quaternary Science Reviews 121, 75-88.

Stevens, T., Buylaert, J.-P., Murray, A.S., 2009. Towards development of a broadly-applicable SAR TT-OSL dating protocol for quartz. Radiation Measurements 44, 639–645.

Terradillos-Bernal, M., Díez Fernández-Lomana, C.J., Jordá-Pardo, J.-F., Benito-Calvo, A., Clemente, I., Marcos-Saiz, J.F., 2017. San Quirce (Palencia, Spain). A Neanderthal open air campsite with short term-occupation patterns. Quaternary International 435, 115-128.

Tsukamoto, S., Duller, G.A.T., Wintle, A.G., 2008. Characteristics of thermally transferred optically stimulated luminescence (TT-OSL) in quartz and its potential for dating sediments. Radiation Measurements 43, 1204–1218.

Wang, X.L., Wintle, A.G., Lu, Y.C., 2006. Thermally transferred luminescence in fine-grained quartz from Chinese loess: Basic observations. Radiation Measurements 41, 649-658.

		Single-grain OSL							Single-grain TT-OSL						
Sample	LU [a]	Grain size (µm) [b]	Total dose rate (Gy/ka)	Accepted/ measured grains [c]	Overdisper-sion (%) [d]	Age Model [d]	D_e (Gy) [f]	Age (ka) [f,g]	Grain size (µm) [b]	Total dose rate (Gy/ka)	Accepted/ measured grains [c]	Overdisper-sion (%) [d]	Age Model [d,e]	D_e (Gy) [f]	Age (ka) [f,g]
Excavation GE-II															
GE16-6	1	212-250	1.88 ± 0.09	80/1400	26 ± 4	CAM	132 ± 5	**70 ± 5**	90-125	1.97 ± 0.09	43/1400	45 ± 7	CAM	169 ± 14	86 ± 8
													MAM-3	*115 ± 15*	*58 ± 8*
													MAM-4	*110 ± 21*	*56 ± 11*
GE16-7	2	212-250	1.82 ± 0.09	79/900	30 ± 4	CAM	145 ± 6	**79 ± 5**	90-125	1.91 ± 0.10	35/700	21 ± 8	CAM	161 ± 10	84 ± 7
Excavation GE-I															
GE16-2	1	212-250	1.22 ± 0.06	52/1300	20 ± 4	CAM	97 ± 4	**80 ± 5**							
GE16-1	2	212-250	1.53 ± 0.08	94/1700	26 ± 3	CAM	127 ± 5	**83 ± 5**	90-125	1.61 ± 0.08	28/1100	20 ± 6	CAM	198 ± 13	123 ± 10
GE16-3	2	212-250	0.75 ± 0.04	53/900	21 ± 4	CAM	85 ± 4	**113 ± 8**							
GE16-4	3	250-300	1.04 ± 0.06	62/700	26 ± 4	CAM	111 ± 5	**107 ± 8**	250-300	1.04 ± 0.06	14/1400	18 ± 12	CAM	131 ± 13	126 ± 14
GE16-5	4	212-250	1.13 ± 0.06	101/1500	22 ± 3	CAM	126 ± 4	**112 ± 7**							

[a] LU = Lithostratigraphic unit
[b] Measurements were made on single-grain discs containing 300 x 300 µm grain-hole positions. The number of grains contained in each grain-hole position is expected to be as follows: 90-125 µm grains = 18 grains per hole; 212-250 µm grains = 1-2 grains per hole; 250-300 µm grains = 1 grains per hole (Arnold et al., 2012).
[c] Number of D_e measurements that passed the SAR rejection criteria / total number of grains or multi-grain aliquots analysed.
[d] CAM = central age model; MAM-3 = three-parameter minimum model; MAM-4 = four-parameter minimum age model (Galbraith et al., 1999); Overdispersion parameter has been calculated using the CAM.
[e] MAM-3 and MAM-4 D_e estimates have been calculated after adding, in quadrature, a relative error of 15% to each individual D_e measurement error to approximate underlying dose overdispersion observed in typical sedimentary samples (Arnold and Roberts, 2009; Arnold et al., submitted).
[f] Mean ± total uncertainty (68% confidence interval), calculated as the quadratic sum of the random and systematic uncertainties.
[g] Total uncertainty includes a systematic component of ±2% associated with laboratory beta-source calibration.

Table 1. Single-grain OSL ages for Galería de las Estatuas. Also shown are the comparative single-grain TT-OSL ages obtained for four of the samples. Ages shown in bold have been used to derive the final chronologies for each sample (see main text for further discussions).


(A)
Galería de las Estatuas
(Atapuerca)
Madrid
Lisbon
N
300 km
Google Earth

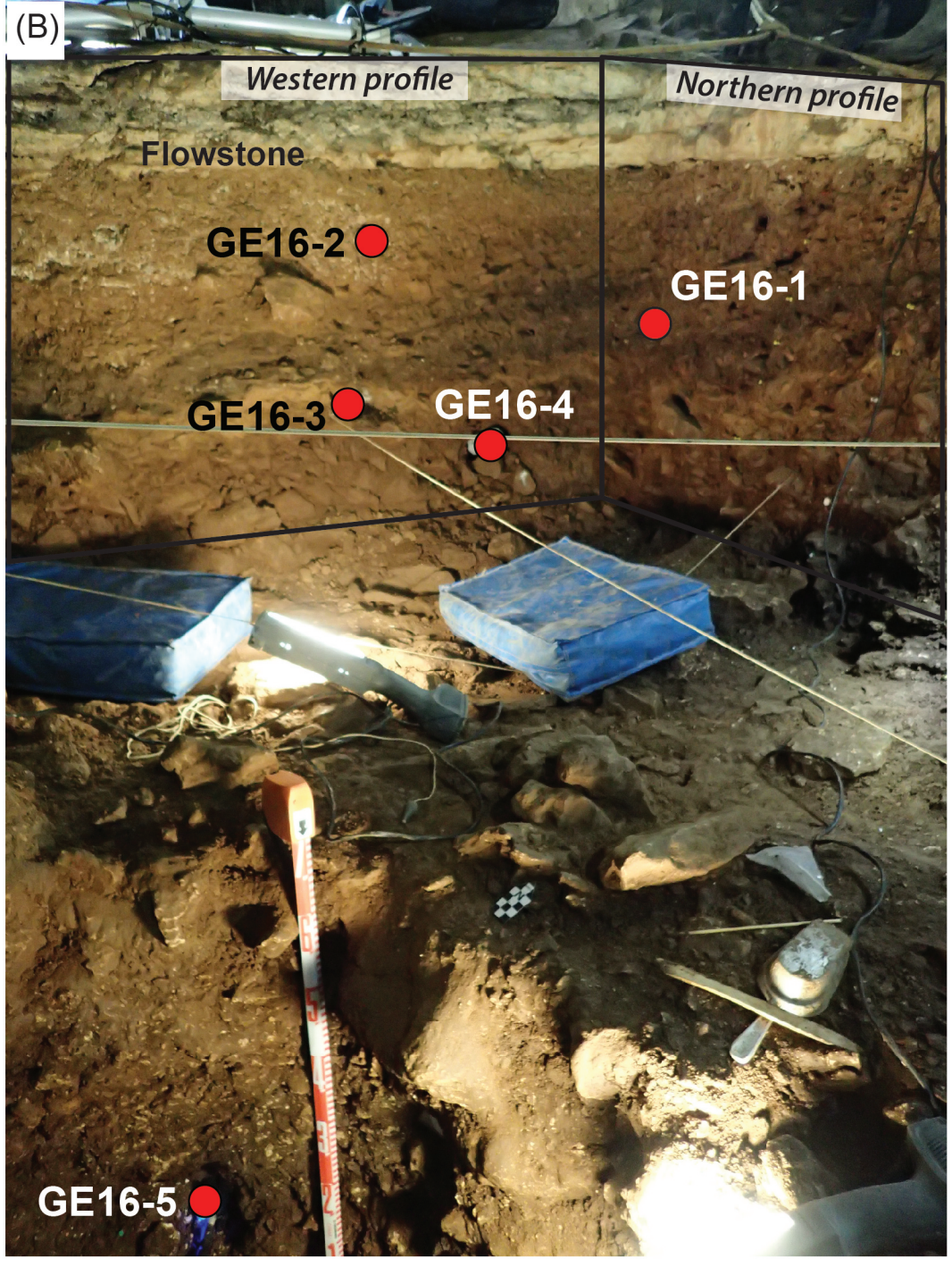
(B)
Western profile
Northern profile
Flowstone
GE16-2
GE16-1
GE16-3
GE16-4
GE16-5


(C)
GE16-6
GE16-7

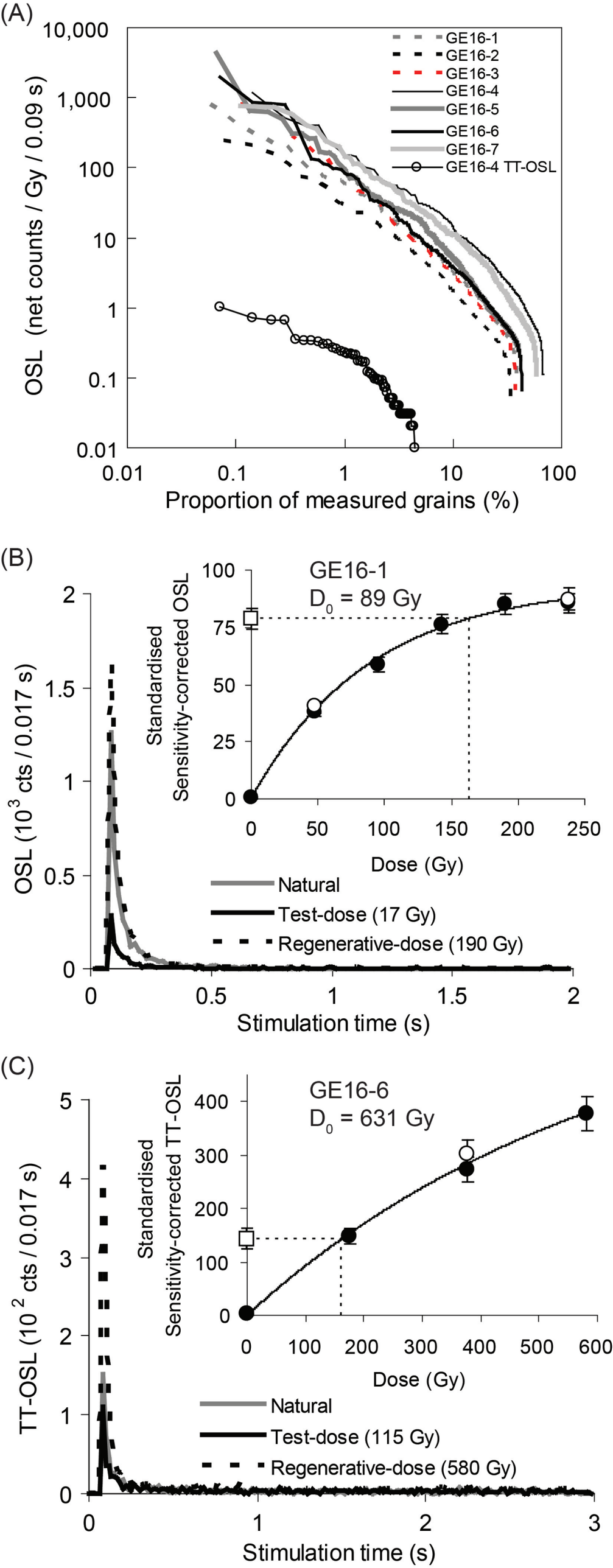
(A)
OSL (net counts / Gy / 0.09 s)
Proportion of measured grains (%)
GE16-1
GE16-2
GE16-3
GE16-4
GE16-5
GE16-6
GE16-7
GE16-4 TT-OSL
(B)
OSL (10^3 cts / 0.017 s)
Stimulation time (s)
GE16-1
D_0 = 89 Gy
Standardised Sensitivity-corrected OSL
Dose (Gy)
Natural
Test-dose (17 Gy)
Regenerative-dose (190 Gy)
(C)
TT-OSL (10^2 cts / 0.017 s)
Stimulation time (s)
GE16-6
D_0 = 631 Gy
Standardised Sensitivity-corrected TT-OSL
Dose (Gy)
Natural
Test-dose (115 Gy)
Regenerative-dose (580 Gy)

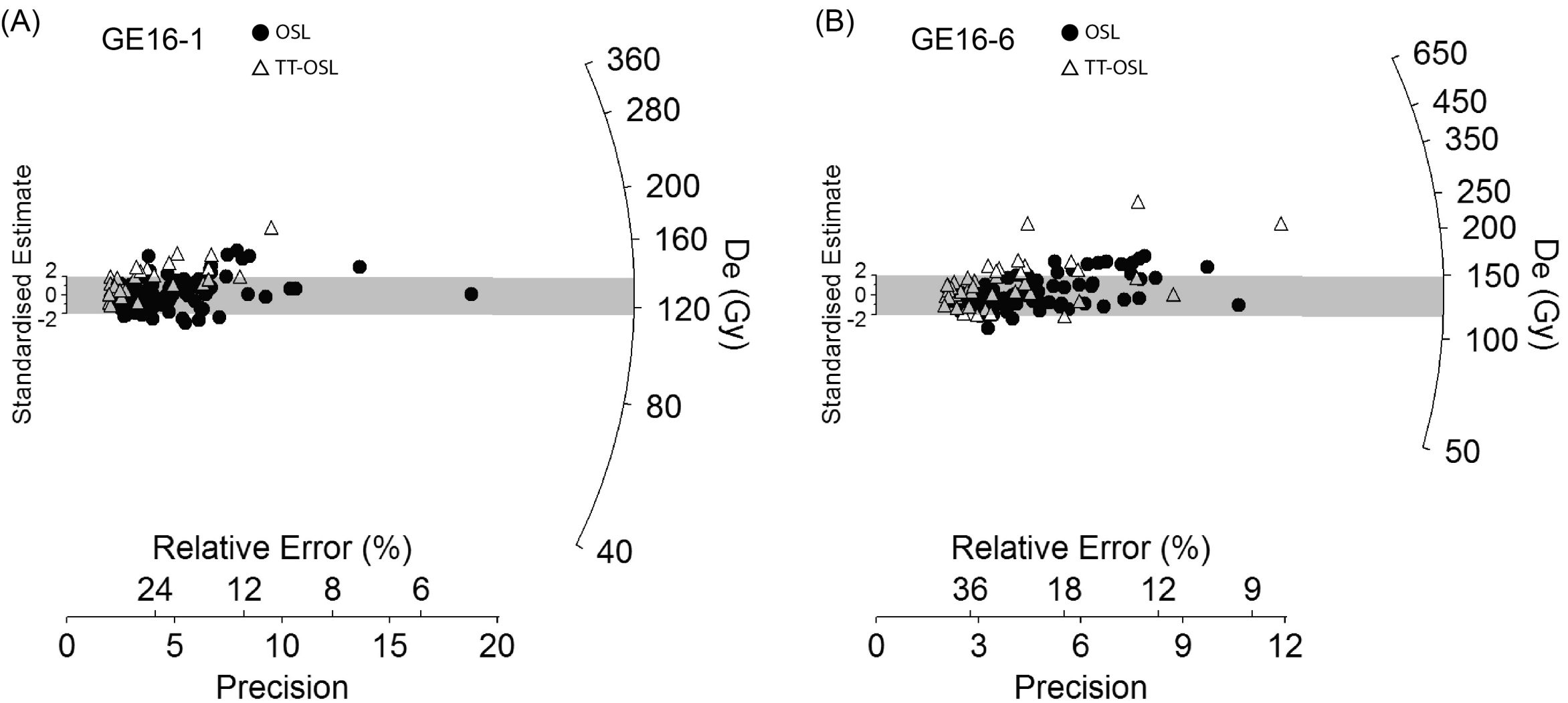
(A)
GE16-1
OSL
TT-OSL
Standardised Estimate
2
0
-2
360
280
200
160
120
80
40
De (Gy)
Relative Error (%)
24
12
8
6
0
5
10
15
20
Precision
(B)
GE16-6
OSL
TT-OSL
Standardised Estimate
2
0
-2
650
450
350
250
200
150
100
50
De (Gy)
Relative Error (%)
36
18
12
9
0
3
6
9
12
Precision

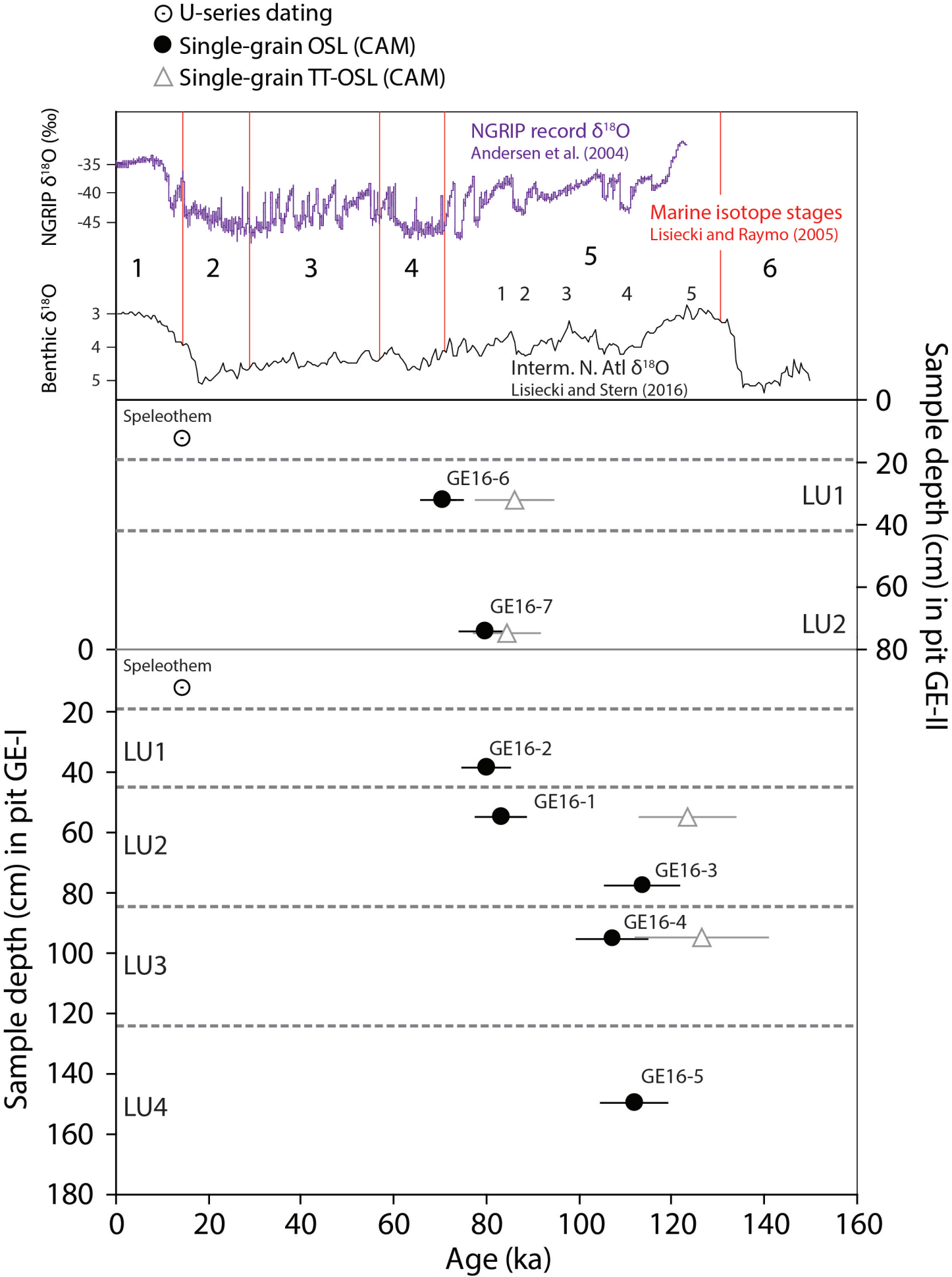
U-series dating
Single-grain OSL (CAM)
Single-grain TT-OSL (CAM)
NGRIP record δ18O
Andersen et al. (2004)
NGRIP δ18O (‰)
-35
-40
-45
Marine isotope stages
Lisiecki and Raymo (2005)
1
2
3
4
5
6
Benthic δ18O
3
4
5
Interm. N. Atl δ18O
Lisiecki and Stern (2016)
Speleothem
GE16-6
LU1
GE16-7
LU2
Speleothem
LU1
GE16-2
GE16-1
LU2
GE16-3
GE16-4
LU3
GE16-5
LU4
Sample depth (cm) in pit GE-I
Sample depth (cm) in pit GE-II
Age (ka)
0
20
40
60
80
100
120
140
160
180

Demuro et al. – Single-grain OSL dating of the Middle Palaeolithic site of Galería de las Estatuas, Atapuerca (Burgos, Spain)

Supplementary Information

Sedimentary sequence

Two sedimentary sequences exposed in separate excavation pits (GE-I and GE-II; located ~ 6 m apart) have been dated in this study (**Figure 1**). The lithostratigraphic units (LU) described for each excavation pit (see below) have been independently assigned and are not necessarily correlative due to lateral variations in sediment composition and differences in the position of the two pits relative to the cave opening (see Arsuaga et al., 2017 for further details).

The ~2 m-deep excavated sequence at GE-I comprises a 1.5–1.75 m-thick allochthonous sedimentary deposit capped by a 20 cm-thick stalagmitic speleothem. The sequence is sub-divided into five LUs, which are ordered, from the base upwards, as follows: LU5 – primarily comprises degraded speleothem fragments; LU4 (~60 cm thick) – composed of dark clays with heterometric angular clasts (cobble size >10 cm); LU3 (~40 cm thick) – composed of orange silty-clays, which become increasingly brown in colour and contain decimetric planar clasts towards the base. These deposits transition into sub-rounded, pebble-supported debris with a silty-clay matrix towards the top; LU2 (~20 cm thick) – made up of dark clays with orange sublevels and more clasts at the base; and LU1 (15-20 cm thick) – composed of orange clays and small (<1 cm diameter) pebbles.

Excavation pit GE-II, located closer to the ancient cave entrance, is ~1.5 m deep and the top 20 cm is made up of the same stalagmitic speleothem present in GE-I. Only two LUs have been identified in the GE-I sedimentary sequence: LU 2 – composed of dark clays with abundant angular planar-clasts (>10 cm long); and LU1 (~30 cm thick) – composed, from the base upwards, of orange clays and sporadic clasts (>10 cm long), and light sands with altered white clasts (possibly speleothem fragments).

In total, seven luminescence dating samples were collected from the sedimentary deposits exposed in pits GE-I and GE-II at Galería de las Estatuas. In pit GE-I, a single sample was collected from each of LU4 and LU3 (GE16-5 and GE16-4, respectively); two samples were collected from the base and upper half of LU2 (GE16-3 and GE16-1, respectively); and one sample was collected from the middle of LU1 (GE16-2). In pit GE-II, one sample was collected from LU1 (GE16-6) and a second sample was taken from LU2 (GE16-7).

Instrumentation and dose rate estimation

Purified coarse-grained quartz fractions were prepared for burial dose estimation using standard preparation procedures (Aitken, 1998), including a 48% HF etch for 40 mins to remove the alpha-irradiated outer layer of the quartz extracts. Single-grain OSL measurements were performed on 212-250 μm quartz grains for all seven samples. Additional single-grain TT-OSL measurements were made on selected samples using either the 90-125 μm (GE16-1, GE16-6 and GE16-7) or 250-300 μm quartz grain fractions (GE16-4), depending on grain-size availability. OSL and TT-OSL signals have been measured on a Risø TL/OSL-DA-20 reader equipped with a a 10 mW Nd:YVO_4 (532 nm) single-grain laser attachment, an EMI 9235QB PMT and a spatially calibrated ^{90}Sr / ^{90}Y β source (~6.7 Gy / min). Single-grain OSL and TT-OSL UV emissions were detected through a 7.5 mm-thick U-340 Hoya filter. All single-grain D_e measurements in this study have been made using standard single-grain aluminium discs drilled with an array of 300 μm x 300 μm holes. It is expected that ~18 grains were placed in each grain-hole position of the single-grain discs when undertaking TT-OSL measurements on the 90-125 μm quartz fractions of samples GE16-1, GE16-6 and GE16-7 (Arnold et al., 2012a). Arnold et al. (2014) and Demuro et al (2014) have shown that the Atapuerca infill deposits contain relatively low proportions of TT-OSL-producing quartz grains. We have therefore chosen to measure the 90-125 μm fractions of these samples to enhance the number of usable grains per disc while minimising any 'pseudo' single-grain

averaging effects. The feasibility of this approach is supported by the TT-OSL grain rejection statistics for sample GE16-4, which were obtained at the true single-grain resolution (i.e., by loading 212-250 μm quartz into the 300 μm x 300 μm grain hole positions). For this sample, only 19% of individually measured grains produced a statistically distinguishable TT-OSL T_n signal (**Table S6**). Demuro et al. (2013) have shown that pseudo single-grain D_e measurements are not likely to induce any significant grain-hole averaging effects for samples characterised by such low yields (<30%) of luminescent grains.

Environmental dose rates (**Table S1**) have been calculated using a combination of in situ gamma spectrometry and low-level beta counting. Concentrations of K, U and Th were determined from field gamma spectra using the 'energy windows' method (Arnold et al., 2012b) and external gamma dose rates were calculated using the conversion factors of Guerin et al. (2011). The external beta dose rates were calculated from measurements made on a Risø GM-25-5 beta counter, using homogenised sediment sub-samples collected from the main luminescence dating sample positions. Cosmic-ray dose rates have been calculated using the approach described in Prescott and Hutton (1994) after taking into consideration site altitude, geomagnetic latitude, and density, thickness and geometry of sediment and bedrock overburden. The beta, gamma and cosmic-ray dose rates have been corrected for long-term sediment moisture contents (Aitken, 1985), which are taken to be equivalent to the present-day measured water contents. The latter ranged between 8% and 28% of dry weight, and have been assigned a relative uncertainty of 20% to accommodate any minor variations in hydrologic conditions during burial.

High-resolution gamma spectrometry (HRGS) was additionally performed on all samples to assess the state of secular equilibrium in the ^{238}U and ^{232}Th decay series (**Table S2**). Daughter-parent isotopic ratios for ^{238}U, ^{226}Ra, ^{210}Pb, ^{228}Ra and ^{228}Th are consistent with unity at either 1σ or 2σ for samples GE16-1, GE16-2, GE16-5, GE16-6 and GE16-7, confirming that the ^{238}U and ^{232}Th chains are in present-day secular equilibrium. For samples GE16-3 and GE16-4, there is evidence for disequilibrium in the upper part of the ^{238}U decay chain, as the ^{226}Ra:^{238}U ratios do not overlap with unity at 2σ (0.71 ± 0.13 and 0.57 ± 0.15, respectively). This disequilibrium may reflect the uptake of unsupported ^{238}U following burial (potentially related to the incorporation of bones in the sediment deposits). Alternatively, since we have used the post-radon daughter emissions of ^{214}Pb and ^{214}Bi to derive ^{226}Ra activities, the apparent excess of ^{238}U with respect to ^{226}Ra may reflect loss of radon (^{222}Rn) gas to the cave atmosphere. Additional insights into the likely cause of this uranium series disequilibrium can be gleaned from the lithogenic ^{230}Th:^{232}Th ratios for these two samples (approximated from the measured ^{238}U:^{228}Ra ratios, assuming equilibrium between ^{238}U and ^{230}Th at the head of the uranium decay series, and assuming equilibrium between ^{232}Th and ^{228}Ra at the head of the thorium decay series). The deposits preserved at Galería de las Estatuas are expected to have broadly similar ^{230}Th:^{232}Th ratios, all else being equal, since they are thought to have originated from a common sediment source (see justification in Olley et al., 1997). This expectation is confirmed for samples GE16-1, GE16-2, GE16-5, GE16-6 and GE16-7, which exhibit a relatively narrow range of ^{230}Th:^{232}Th (^{238}U:^{228}Ra) ratios (0.8 to 1.3). In contrast, samples GE16-3 and GE16-4 exhibit significantly higher ^{238}U:^{228}Ra values (2.3), consistent with the uptake of additional, unsupported parental ^{238}U at the head of the uranium decay series. This interpretation is further supported by considering the ^{226}Ra:^{228}Ra ratios of samples GE16-3 and GE16-4 as a proxy for their lithogenic ^{230}Th:^{232}Th ratios. Using this alternative assessment, the two samples yield ^{230}Th:^{232}Th ratios of 1.3 – 1.6, which are in closer agreement with the ^{230}Th:^{232}Th ratios of the five samples that are in present-day secular equilibrium.

The excess ^{238}U activities of samples GE16-3 and GE16-4 are not considered to have a significant effect on the final dose rate estimates, as borne out by the stratigraphic consistency of the single-grain OSL ages obtained for excavation pit GE-I (see main text and **Figure 4**). Dosimetry modelling studies undertaken elsewhere have demonstrated that isotopic disequilibria of similar magnitudes are only likely to give rise to minor deviations (<5%) in long-term dose rate estimates (e.g., Olley et al., 1996, 1997; Preusser and Degering, 2007). Such systematic biases would be significantly less than the existing uncertainty ranges on our final dose rate estimates. The effects of ^{238}U disequilibrium will be further diminished for samples

GE16-3 and GE16-4 because the ^{238}U decay series only contributes 33-36% to the total quartz dose rate (calculated using the high resolution gamma spectrometry results). In this study, the gamma dose rates of the ^{238}U series have also been derived from post-radon emissions of ^{214}Bi daughter isotopes using field gamma spectrometry. This approach is likely to provide a more accurate assessment of the present-day dose rate if secular disequilibrium has occurred at the head of the decay series because ~98% of the ^{238}U series gamma dose rate originates from post-radon decays in the lower part of the chain (namely ^{226}Ra and its daughters; Stokes et al. 2003). Similarly, the beta counting results obtained in this study are not critically dependent on the assumption of ^{238}U secular equilibrium because ~60% of the beta particle emissions measured in the uranium decay series will have originated from ^{226}Ra and its daughters near the bottom of the decay chain.

Equivalent dose (D_e) measurements and estimation

Single-grain OSL and TT-OSL D_e measurements were made using the single-aliquot regenerative-dose (SAR) protocols described in Murray and Wintle (2000) and Stevens et al. (2009), respectively, which were modified to enable measurements of individual grains (e.g., Arnold et al., 2016; Demuro et al., 2014; **Table S3**. Single grain OSL and TT-OSL D_e values were calculated after interpolating the sensitivity-corrected natural signal onto a sensitivity-corrected dose response curve that had been fitted with a single saturating exponential function. In all cases, the characteristic saturation dose (D_0) value of the saturating exponential dose response curve was calculated for each grain. Sensitivity-corrected OSL and TT-OSL responses were constructed from the first 0.09 s and 0.24 s of laser stimulation, respectively, with a background subtraction derived from the last 0.25 s of stimulation. Individual D_e uncertainty ranges comprise from three sources of error: (i) a random uncertainty term arising from photon counting statistics for each OSL or TT-OSL measurement, calculated using Eq. 3 of Galbraith (2002); (ii) an empirically determined instrument reproducibility uncertainty of 1.9% for each single-grain measurement (calculated for the specific Risø reader used in this study according to the approach outlined in Jacobs et al., 2006a); and (iii) a dose-response curve fitting uncertainty determined using 1000 iterations of the Monte Carlo method described by Duller (2007) and implemented in Analyst.

Single-grain OSL and TT-OSL D_e estimates were not considered suitable for final age calculation if they exhibited one or more of the following properties: (i) their net T_n signals were $<3\sigma$ above the late-light background; (ii) recycling ratios (sensitivity-corrected luminescence responses (L_x/T_x) for two identical regenerative doses) were not consistent with unity at 2σ. For the single-grain OSL measurements, the recycling ratio test was performed using both a low-dose and high-dose regenerative dose cycle; (iii) the OSL-IR depletion ratio (Duller, 2003) was less than unity at 2σ; (iv) the recuperation ratio, calculated as the ratio of the sensitivity-corrected 0 Gy dose point (L_0/T_x) to the sensitivity-corrected natural (L_n/T_n), was >5%; (v) the net T_n signal had a relative error of >30%; (vi) the sensitivity-corrected natural signal (L_n/T_n) did not intercept the sensitivity-corrected dose-response curve; (vii) the dose-response curve displayed anomalous properties (i.e., zero or negative response with increasing dose) or very scattered L_x/T_x values that could not be successfully fitted with the Monte Carlo procedure and, hence, did not yield finite D_e values and uncertainty ranges; (viii) the L_n/T_n value intercepted the saturated part of the dose-response curve (L_n/T_n values were equal to the I_{max} saturation limit of the dose-response curve at 2σ). The single-grain OSL and TT-OSL rejection statistics for the measured samples are shown in **Table S5** and **Table S6**, respectively. Additionally, during analysis of the single-grain TT-OSL datasets it was found that a number of initially accepted grains displayed non-negligible, slow-decaying TT-OSL signals (i.e., their T_x signals did not reach background after 2 s of laser stimulation). Further examination showed that the signals of these grains did not originate from genuine thermal transfer of charge into the fast OSL trap, but rather they corresponded to interfering (non-transferred) slow OSL components from the previous OSL stimulation, which had not reached background levels prior to commencing the TT-OSL measurements. As such these grains were not included in the final D_e estimation, and they have been assigned to an additional TT-OSL rejection category in **Table S6**.

It is noteworthy that 3-12% of measured single-grain OSL D_e values were rejected because their sensitivity-corrected natural signals intercepted the saturated region of their corresponding sensitivity-corrected dose response curves. If these rejected D_e values relate to genuinely old grains that are in dose saturation, then their exclusion may have acted to artificially truncate the upper tails of our empirical D_e distributions. However, there is reasonable evidence to suggest that these rejected saturated grains reflect intrinsically unfavourable OSL characteristics and / or non-optimal grain responses to the D_e measurement procedure. In particular, these rejected saturated grain populations exhibit below-average dose saturation characteristics, which are significantly lower than the corresponding dose saturation ranges observed for the accepted grains. The majority (70%) of rejected saturated grains have D_0 values of <50 Gy (**Figure S5**). The CAM D_0 value calculated for these rejected grains is 42 ± 1 Gy (n = 372), which is 50% lower than the mean D_0 value of accepted grains. The dose recovery and natural D_e datasets of GE16-1 also share similar proportions of saturated grains (3-5%), confirming that these behaviours are not exclusive to natural burial dose measurements. Taken together, these observations suggest that the rejected saturated grain populations have an experimental origin and that they may reflect unfavourable grain responses to the chosen SAR protocols. The exclusion of these grain populations from the final D_e datasets is therefore warranted and unlikely to exert any undue effects on the single-grain OSL age calculations.

Single-grain OSL and TT-OSL dose recovery tests were undertaken on samples GE16-1 and GE16-7, respectively, to assess the suitability of the chosen SAR protocols. Single-grain OSL dose recovery test measurements were made after administering a dose of 100 Gy to grains that had previously been bleached with two exposures of 1,000 s to blue LEDs, separated by a 10,000 s pause. Regenerative dose and test dose preheat treatments of 240°C for 10 s and 160°C for 10 s, respectively, were used in the single-grain dose recovery test (**Figure S2**). These preheat conditions were determined to be optimal for sample GE16-1 from initial multi-grain OSL dose recovery tests (**Figure S3**), which were conducted using blue LED OSL stimulation instead of green laser stimulation in steps 4 and 7 of the SAR sequence shown in **Table S3a**. The single-grain TT-OSL dose recovery tests were performed on GE16-7 by adding a dose of 148 Gy on top of the naturally accumulated dose for a sub-set of grains. This approach was adopted owing to the long durations of light exposure needed to bleach natural TT-OSL signals down to low residual levels. The recovered dose ratio was then calculated by subtracting the weighted mean natural D_e of sample GE16-7 from the weighted mean D_e of the unbleached and dosed grains (**Table S4**). Single-grain OSL and TT-OSL measured-to-given dose ratios of 0.98 ± 0.03 and 1.12 ± 0.14 were obtained using these procedures. Both dose recovery ratios are within 2σ of unity, and support the suitability of the D_e measurement conditions used in this study.

References

Aitken, M.J., 1985. Thermoluminescence Dating. Academic Press, London, 359 p.

Aitken 1998. An Introduction to Optical Dating: The Dating of Quaternary Sediments by the Use of Photon-Stimulated Luminescence. Oxford University Press, Oxford, 267 p.

Arnold, L.J., Demuro, M., Navazo Ruiz, M., 2012a. Empirical insights into multi-grain averaging effects from 'pseudo' single-grain OSL measurements. Radiation Measurements 47, 652-658.

Arnold, L.J., Duval, M., Falguères, C., Bahain, J.-J., Demuro, M., 2012b. Portable gamma spectrometry with cerium-doped lanthanum bromide scintillators: suitability assessments for luminescence and electron spin dating applications. Radiation Measurements 47, 6-18.

Arnold, L.J., Demuro, M., Navazo Ruiz, M., Benito-Calvo, A., Pérez-González, A., 2013. OSL dating of the Middle Palaeolithic Hotel California site, Sierra de Atapuerca, north-central Spain. Boreas 42, 285-305.

Arnold, L.J., Demuro, M., Parés, J.M., Arsuaga, J.L., Aranburu, A., Bermúdez de Castro, J.M., Carbonell, E., 2014. Luminescence dating and palaeomagnetic age constraint on hominins from Sima de los Huesos, Atapuerca, Spain. Journal of Human Evolution 67, 85-107.

Arnold, L.J., Duval, M., Demuro, M., Spooner, N.A., Santonja, M., Pérez-González, A., 2016. OSL dating of individual quartz 'supergrains' from the Ancient Middle Palaeolithic site of Cuesta de la Bajada, Spain. Quaternary Geochronology 36, 78-101.

Arsuaga J.L., Baquedano, E., Pérez-González, A., Sala, N., Quam, R.M., Rodríguez, L., García, R., García, N., Alvarez-Lao, D.J., Laplana, C., Huguet, R., Sevilla, P., Maldonado, E., Blain, H-A., Ruiz-Zapata, M.B., Sala, P., Gil-García, J., Uzquiano, P., Pantoja, A., Márquez, B., 2012. Understanding the ancient habitats of the last interglacial (late MIS 5) Neanderthals of central Iberia: Paleoenvironmental and taphonomic evidence from the Cueva del Camino (Spain) site. Quaternary International 275, 55-75.

Arsuaga, J.L., Gómez-Olivencia, A., Sala, N., Martínez-Pillado, V., Pablos, A., Bonmatí, A., Pantoja-Pérez, A., Lira-Garrido, J., Alcázar de Velasco, A., Ortega, A.I., Cuenca-Bescós, G., García, N., Aranburu, A., Ruiz-Zapata, B., Gil-García, M.J., Rodríguez-Alvarez, X.P., Ollé, A., Mosquera, M., 2017. Evidence of paleoecological changes and Mousterian occupations at the Galería de las Estatuas site, Sierra de Atapuerca, norther Iberian plateau, Spain. Quaternary Research 88, 345-367.

Bischoff, J.L., Garcia, J.F., Straus, G., 1992. Uranium-series isochron dating at El Castillo cave (Cantabria, Spain): the "Acheulean"/"Mousterian" question. Journal of Archaeological Science 19, 49-92.

Bowler, J.M., Johnston, H., Olley, J.M., Prescott, J.R., Roberts, R.G., Shawcross, W., Spooner, N.A., 2003. New ages for human occupation and climate change at Lake Mungo, Australia. Nature 421, 837-840.

Bøtter-Jensen, L., Mejdahl, M., 1988. Assessment of beta dose-rate using a GM multicounter system. Nuclear Tracks and Radiation Measurements 14, 187-191.

Brennan, B.J., 2003. Beta doses to spherical grains. Radiation Measurements 37, 299-303.

Bronk Ramsey, C., Lee, S., 2013. Recent and planned developments of the program OxCal, Radiocarbon 55, 3-4.

Dalén, L., Orlando, L., Shapiro, B., Brandström-Durling, M., Quam, R., Thomas, M., Gilbert, P., Díez Fernández-Lomana, J.C., Willerslev, E., Arsuaga, J.L., Gotherström, A., 2012. Partial genetic turnover in Neanderthals: continuity in the east and population replacement in the west. Mol Biol Evol 29, 1893-1897.

Demuro, M., Arnold, L.J., Froese, D.G., Roberts, R.G., 2013. OSL dating of loess deposits bracketing Sheep Creek tephra beds, northwest Canada: Dim and problematic single-grain OSL characteristics and their effect on multi-grain age estimates. Quaternary Geochronology 15, 67-87.

Demuro, M., Arnold, L.J., Parés, J.M., Pérez-González, A., Ortega, A.I., Arsuaga, J.L., Bermúdez de Castro, J.M., Carbonell, E., 2014. New luminescence ages for the Galería Complex archaeological site: Resolving chronological uncertainties on the Acheulean record of the Sierra de Atapuerca, northern Spain. PLOS ONE 9, e110169.

Demuro, M., Arnold, L.J., Parés, J.M., Sala, R., 2015. Extended-range luminescence chronologies suggest potentially complex bone accumulation histories at the Early-to-Middle Pleistocene palaeontological site of Huéscar-1 (Guadix-Baza basin, Spain). Quaternary International 389, 191-212.

Díez, C., Alonso, R., Bengoechea, A., Colina, A., Jordá, J.F., Navazo, M., Ortiz, J.E., Pérez, S., Torres, T., 2008. El Paleolítico Medio en el valle del Arlanza (Burgos), los sitios de La Ermita, Millán y La Mina. Quaternario Geo-morfolgía 22, 135-157.

Diez Martín, F., Sánchez Yustos, P., Gómez González, J A., Gómez de la Rua, D., Yravedra Sáinz de los Terreros, J., Díaz Muñoz, I., 2011. La ocupacion neanderthal en el Canon de La Horadada (Mave, Palencia, España): nuevas perspectivas arqueológicas en Cueva Corazón. Munibe (Antropologia-Arkeologia) 62, 65-85.

Domingo, R., Peña-Monné, J.L., Torres, Y., Ortiz, E.J., Utrilla, P., 2017. Neanderthal highlanders: Las Callejuelas (Monteagudo del Castillo, Teruel, Spain), a high-altitude site occupied during MIS 5. Quaternary International 435, 129-143.

Duller, G.A.T., 2003. Distinguishing quartz and feldspar in single grain luminescence measurements. Radiation Measurements 37, 161–165.

Duller, G.A.T., 2007. Assessing the error on equivalent dose estimates derived from single aliquot regenerative dose measurements. Ancient TL 25, 15-24.

Galbraith, R., 2002. A note on the variance of a background-corrected OSL count. Ancient TL 20, 49-51.

Guérin, G., Mercier, M., Adamiec, G., 2011. Dose-rate conversion factors: update. Ancient TL 29, 5-8.

Jacobs, Z., Duller, G.A.T., Wintle, A.G., 2006a. Interpretation of single grain D_e distributions and calculation of D_e. Radiation Measurements 41, 264-277.

Jacobs, Z., Duller, G.A.T., Wintle, A.G., Henshilwood, C.S., 2006b. Extending the chronology of deposits at Blombos Cave, South Africa, back to 140 ka using optical dating of single and multiple grains of quartz. Journal of Human Evolution 51, 255-273.

Murray, A.S., Wintle, A., 2000. Luminescence dating of quartz using an improved single-aliquot regenerative-dose protocol. Radiation Measurements 32, 57-73.

Martínez-Pillado, V., Aranburu, A., Arsuaga, J.L., Ruiz-Zapata, B., Gil-García, M.J., Stoll, H., Yusta, I., Iriarte, E., Carretero, J.M., Edwards, R.L., Cheng, H., 2014. Upper Pleistocene and Holocene palaeoenvironmental records in Cueva Mayor karst (Atapuerca, Spain) from different proxies: speleothem crystal fabrics, palynology, and archaeology. International Journal of Speleology 43, 1-14.

Mejdahl, V., 1979. Thermoluminescence dating: beta-dose attenuation in quartz grains. Archaeometry 21, 61–72.

Mejdahl, V., 1987. Internal radioactivity in quartz and feldspar grains. Ancient TL 5, 10-17.

Moure, A., García Soto, E., 1982. Datación radiocarbónica del Mousteriense de Cueva Millán (Hortiguela, Burgos). Boletín del Sedimentario de Estudios de Arte y Arqueología 48, 71-72.

Navazo, M., Díez, J.C., Torres, T., Colina, A., Ortiz, J.E., 2005. La cueva de Prado Vargas. Un yacimiento del Paleolítico Medio en el sur de la Cordillera Cantábrica. In: Lasheras, J.A., Montes, R. (Eds.), Neandertales cantábricos, estado de la cuestión. Museo de Altamira, Santander, pp. 151-166.

Navazo, M., Alonso-Alcalde, R., Benito-Calvo, A., Diez, J.C., Perez-Gonzalez, A., Carbonell, E., 2011. Hundidero: MIS 4 open air Neanderthal occupations in Sierra de Atapuerca. Archaeology Ethnology & Anthropology of Eurasia 39, 29-41.

Olley, J.M., Murray, A., Roberts, R.G., 1996. The effects of disequilibria in the uranium and thorium decay chains on burial dose rates in fluvial sediments. Quaternary Science Reviews (Quaternary Geochronology) 15, 751-760.

Olley, J.M., Roberts, R.G., Murray, A.S., 1997. Disequilibria in the uranium decay series in sedimentary deposits at Allen's Cave, Nullarbor Plain, Australia: implications for dose rate determinations. Radiation Measurements 27, 433-443.

Ortega, A.I., Benito-Calvo, A., Pérez-González, A., Martín-Merino, M.A., Pérez-Martínez, R., Pares, J.M., Aramburu, A., Arsuaga, J.L., Bermúdez de Castro, J.L., Carbonell, E., 2013. Evolution of multilevel caves in the Sierra de Atapuerca (Burgos, Spain) and its relation to human occupation. Geomorphology 196, 122-137.

Pawley, S.M., Bailey, R.M., Rose, J., Moorlock, B.S.P., Hamblin, R.J.O., Booth, S.J., Lee, J.R., 2008. Age limits on Middle Pleistocene glacial sediments from OSL dating, north Norfolk, UK. Quaternary Science Reviews 27, 1363-1377.

Prescott, J.R., Hutton, J.T., 1994. Cosmic ray contributions to dose rates for luminescence and ESR dating: large depths and long-term time variations. Radiation Measurements 23, 497-500.

Preusser, F., Degering, D., 2007. Luminescence dating of the Niederweningen mammoth site, Switzerland. Quaternary International 164-165, 106-112.

Quam, R.M., Arsuaga, J.L., Bermúdez de Castro, J.M., Díez, C.J., Lorenzo, C., Carretero, J.M., García, N., Ortega, A.I., 2001. Human remains from Valdegoba Cave (Huérmeces, Burgos, Spain). Journal of Human Evolution 41, 385-435.

Readhead, M.L., 2002. Absorbed dose fraction for ^{87}Rb β particles. Ancient TL 20, 25-28.

Rees-Jones, J., 1995. Optical dating of young sediments using fine-grain quartz. Ancient TL 13, 9-14.

Rees-Jones, J., Tite, M.S., 1997. Optical dating results for British archaeological sediments. Archaeometry 39, 177-187.

Reimer, P.J., Bard, E., Bayliss, A., Beck, J.W., Blackwell, P.G., Bronk Ramsey, C., Buck, C.E., Cheng, H., Edwards, R.L., Friedrich, M., Grootes, P.M., Guilderson, T.P., Haflidason, H., Hajdas, I., Hatté, C., Heaton, T.J., Hoffmann, D.L., Hogg, A.G., Hughen, K.A., Kaiser, K.F., Kromer, B., Manning, S.W., Niu. M., Reimer, R.W., Richards, D.A., Scott, E.M., Southon, J.R., Staff, R.A., Turney, C.S.M., van der Plicht, J., 2013. IntCal13 and Marine13 radiocarbon age calibration curves 0–50,000 years cal BP. Radiocarbon 55, 1869–1887.

Sánchez Yustos, P., Diez Martín, F., 2016. Dancing to the rhythms of the Pleistocene? Early Middle Palaeolithic populations dynamics in NW Iberia (Duero Basin and Cantabrian Region). Quaternary Science Reviews 121, 75-88.

Stevens, T., Buylaert, J.-P., Murray, A.S., 2009. Towards development of a broadly-applicable SAR TT-OSL dating protocol for quartz. Radiation Measurements 44, 639-645.

Stokes, S., Ingram, S., Aitken, M.J., Sirocko, F., Anderson, R., Leuschner, D., 2003. Alternative chronologies for Late Quaternary (Last Interglacial-Holocene) deep sea sediments via optical dating of silt-sized quartz. Quaternary Science Reviews 22, 925-941.

Terradillos-Bernal, M., Díez Fernández-Lomana, C.J., Jordá-Pardo, J.-F., Benito-Calvo, A., Clemente, I., Marcos-Saiz, J.F., 2017. San Quirce (Palencia, Spain). A Neanderthal open air campsite with short term-occupation patterns. Quaternary International 435, 115-128.

Wintle, A.G., Murray, A.S., 2006. A review of quartz optically stimulated luminescence characteristics and their relevance in single-aliquot regeneration dating protocols. Radiation Measurements 41, 369-391.

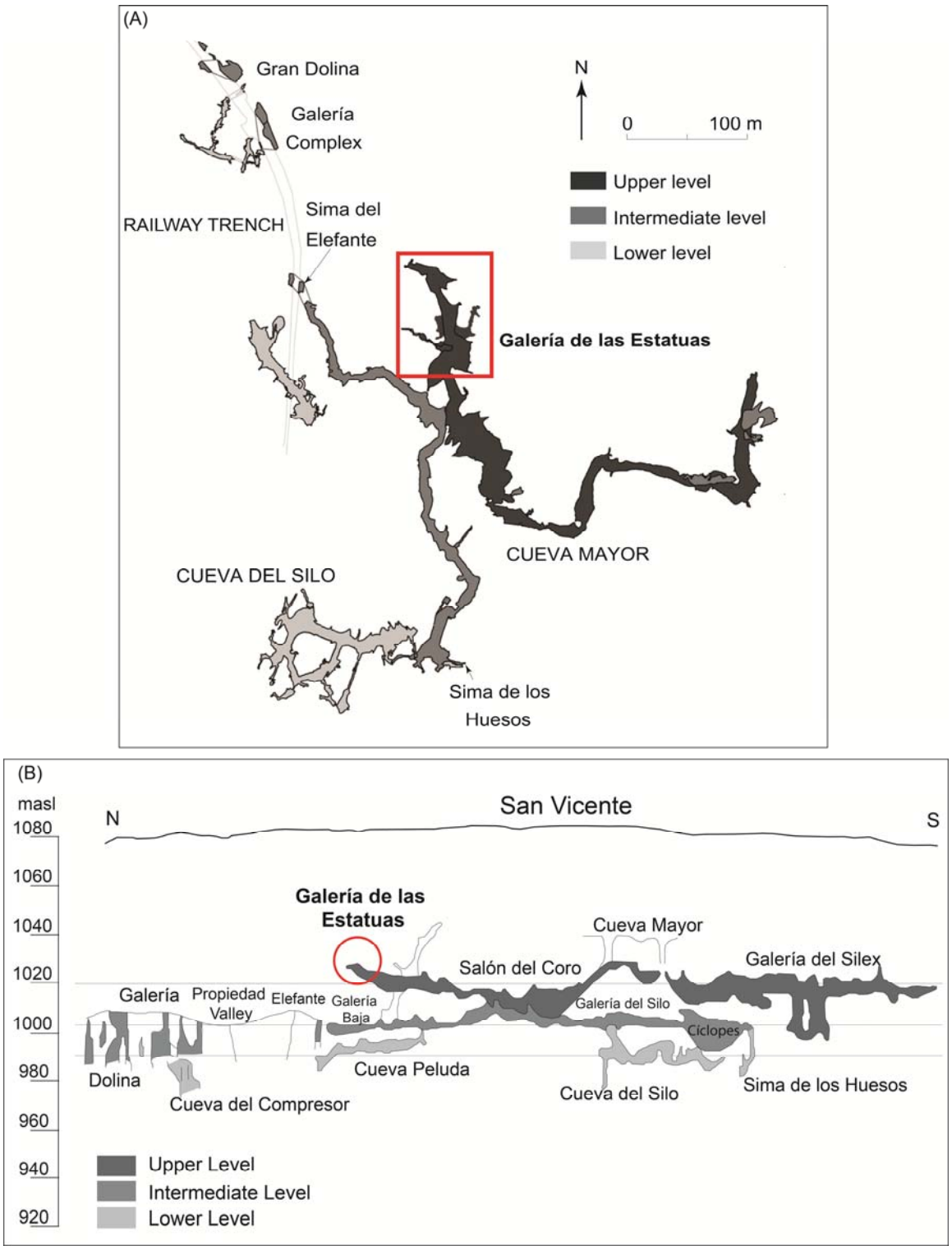

Figure S1. Maps showing the location of the Galería de las Estatuas site within the multi-level Cueva Mayor-Cueva del Silo cave system at Atapuerca (modified from Ortega et al., 2013). (A) Plan view of the endokarst system. The red box highlights the location of Galería de las Estatuas site. (B) Cross-sectional view of the cave system. The red circle highlights the location of Galería de las Estatuas site.

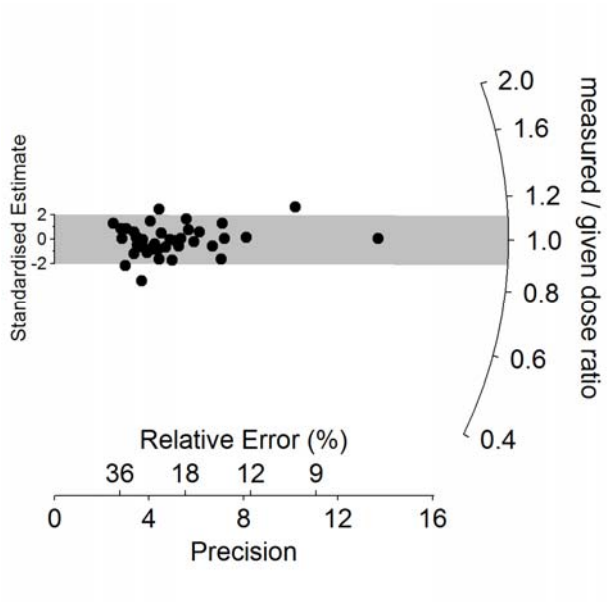

Figure S2. Radial plot showing single-grain OSL dose recovery test results obtained for 212-250 μm quartz grains of sample GE16-1 using SAR protocol A in **Table S3** (D_e errors are shown at 1σ). Grains were bleached within the Risø reader chamber using blue LEDs prior to administering a dose of 100 Gy. The central age model (CAM) measured-to-given dose ratio is 0.98 ± 0.03 and the overdispersion is 10 ± 5%.

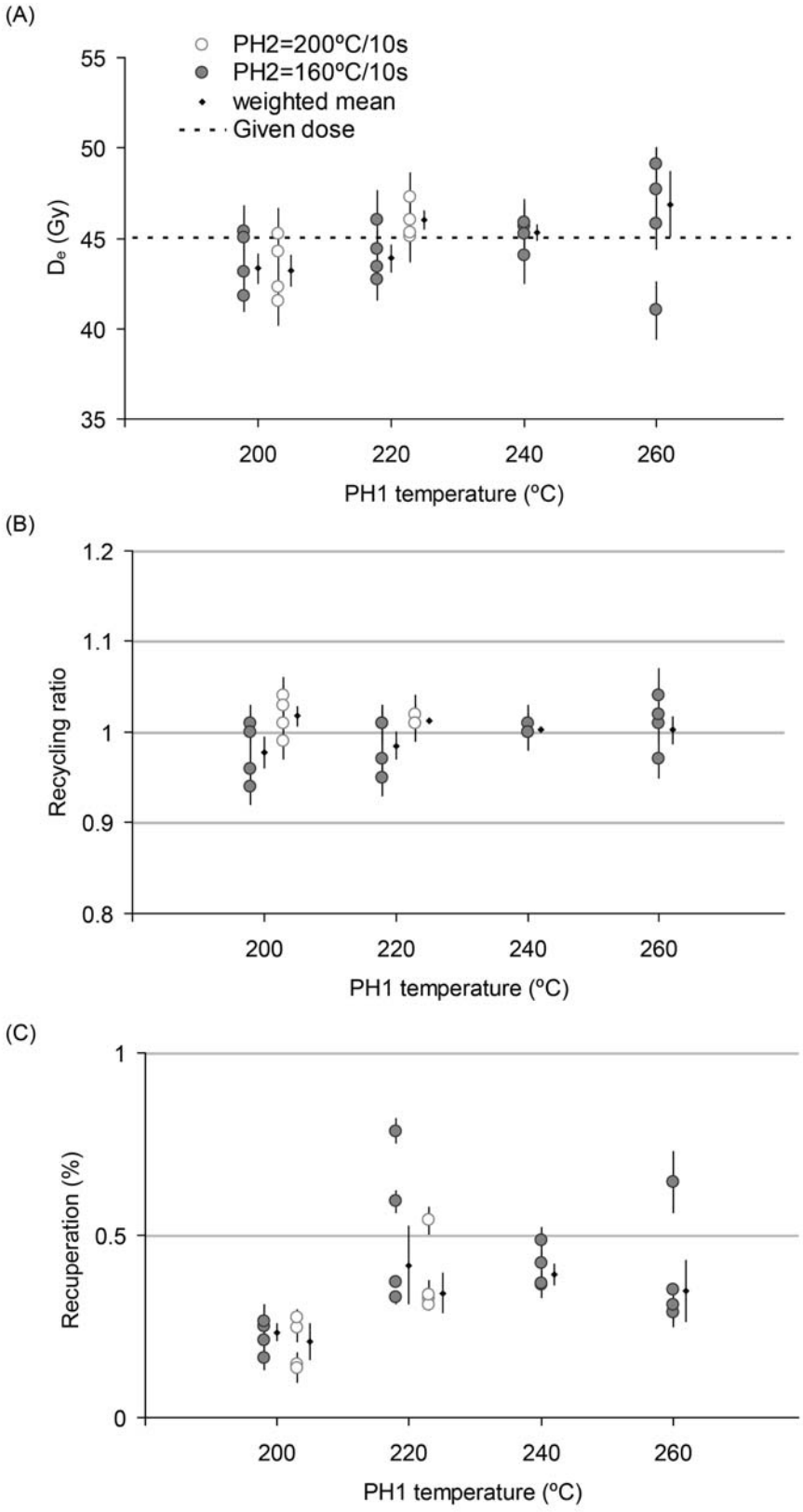

Figure S3. Multi-grain dose recovery test results obtained for sample GE16-1 after administering a dose of 45 Gy (errors are shown at 1σ). Plots show (A) the recovered doses, (B) the recycling ratios and (C) the recuperation values obtained for different preheat conditions. D_e measurements were made with a modified version of SAR protocol A (replacing single-grain laser stimulations in steps 4 and 7 with blue LED OSL stimulations performed at 125 ºC for 60 s) using various regenerative-dose preheat (PH1) and test-dose preheat (PH2) combinations. D_e measurements were made on multi-grain aliquots containing ~900 quartz grains.

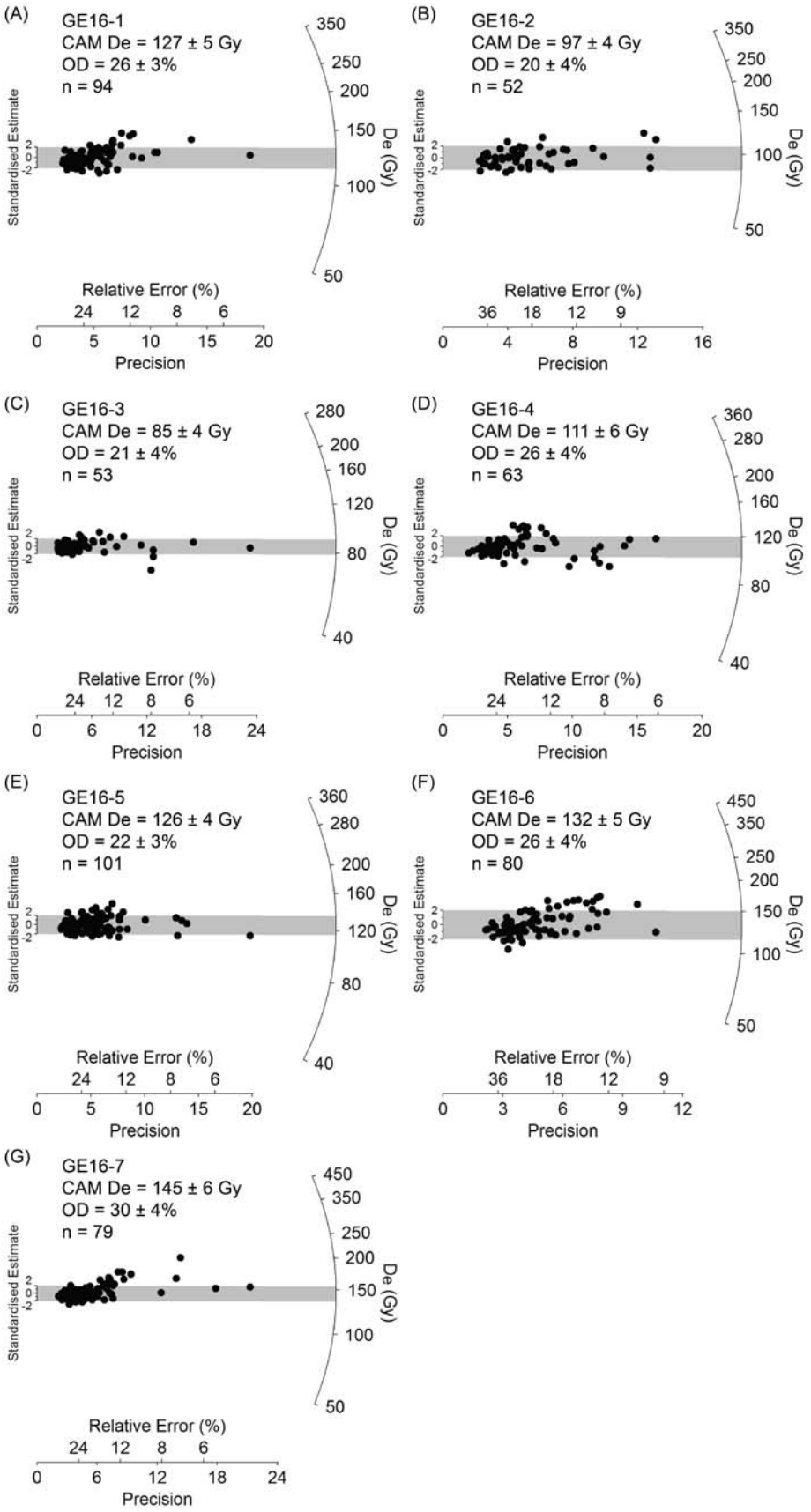

Figure S4. Radial plots showing the single-grain OSL D_e distributions obtained for the Galería de las Estatuas samples (D_e errors are shown at 1σ). The dark grey bands are centred on the weighted mean D_e values, which have been calculated using the CAM.

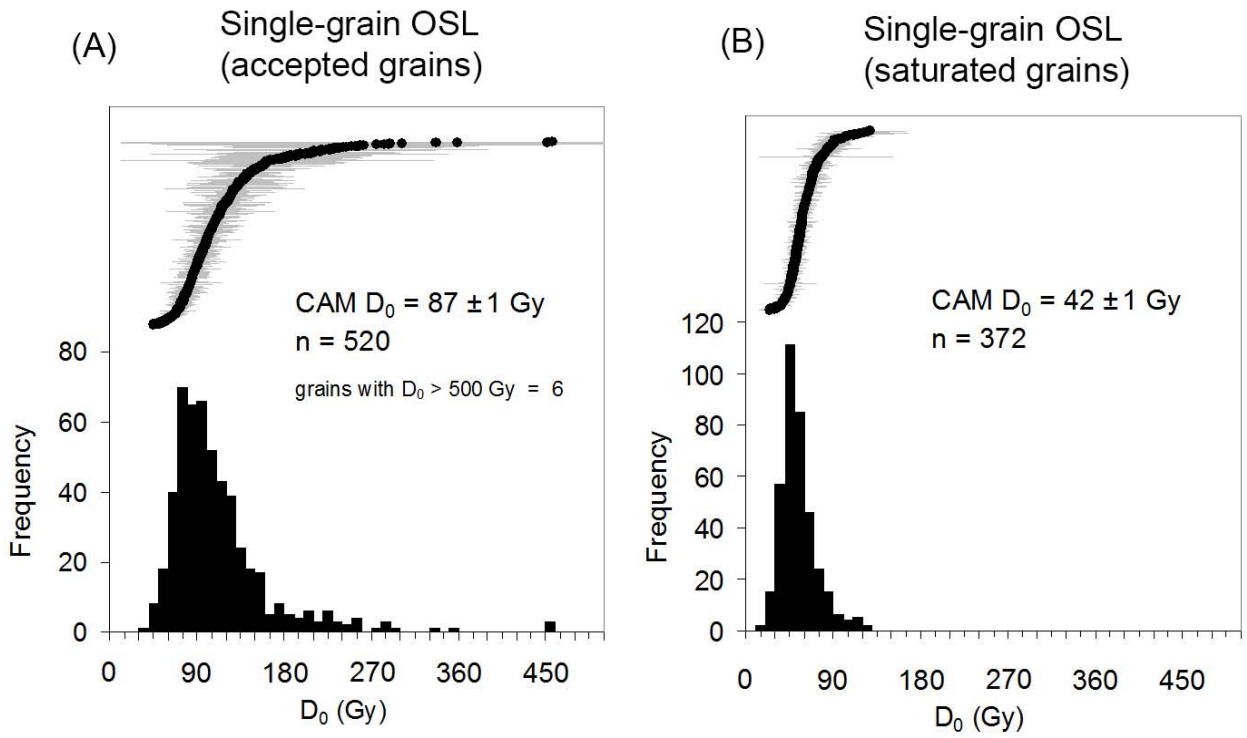

Figure S5. Histograms showing the range of single-grain OSL D_0 values obtained for accepted and saturated grains (D_0 errors are shown at 1σ). The D_0 value characterises the rate of signal saturation with respect to administered dose and equates to the dose value for which the saturating exponential dose-response curve slope is $1/e$ (or ~ 0.37) of its initial value. D_0 values have been calculated using saturating exponential dose response curve fits in all cases.

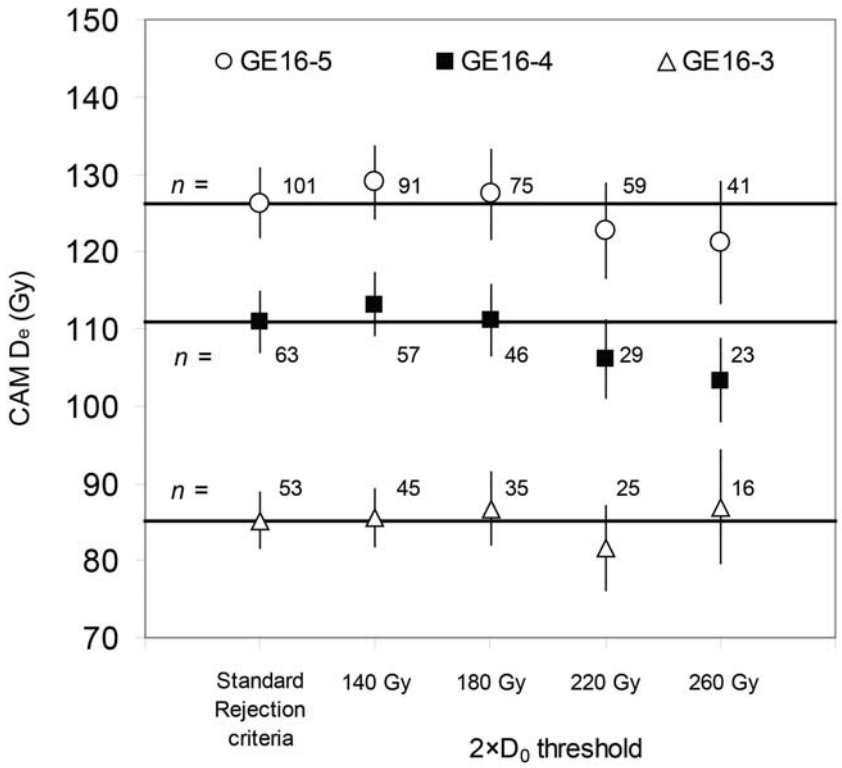

Figure S6. Changes in single-grain CAM D_e values observed after applying the indicated $2*D_0$ threshold values (Demuro et al., 2015; Arnold et al., 2016) to the originally accepted D_e datasets of three representative samples (D_e errors are shown at 1σ). Similar plots were obtained for the remaining samples. The number of accepted grains remaining after applying progressively higher $2*D_0$ thresholds is shown for each sample.

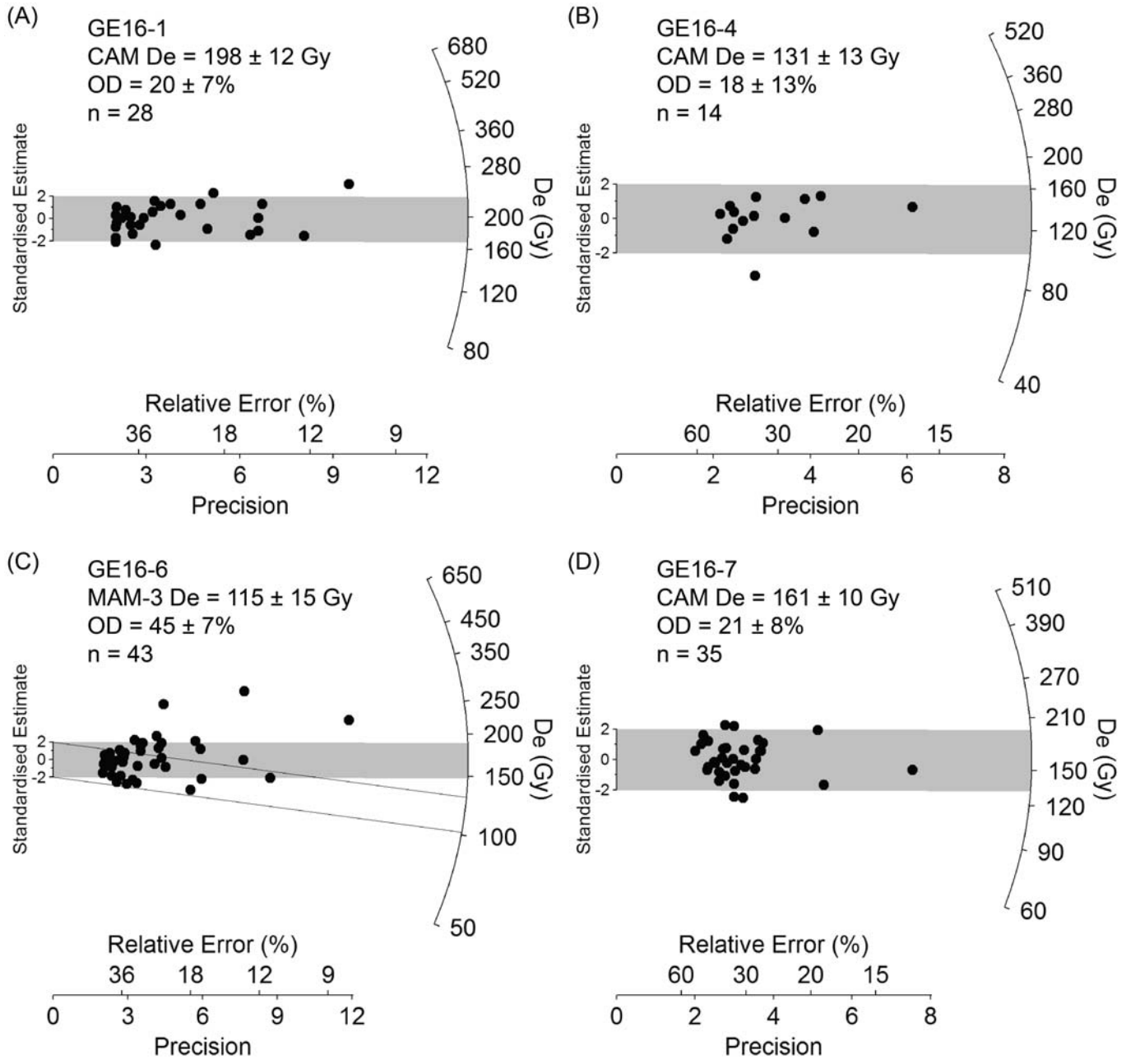

Figure S7. Radial plots showing the single-grain TT-OSL D_e distributions obtained for a subset of the Galería de las Estatuas samples; (A) GE16-1, (B) GE16-4, (C) GE16-6 and (D) GE16-7 (D_e errors are shown at 1σ). The dark grey bands are centred on the weighted mean D_e values, which have been calculated using the CAM. In (C) the open band is centred on the mean D_e obtained using the 3-parameter minimum age model (MAM-3).

Sample	Sample depth (cm)	Water content [a]	Grain fraction (µm)	Gamma dose rate (Gy/ka) [b, c]	Beta dose rate (Gy/ka) [d]	Cosmic dose rate (Gy/ka) [e]	Internal dose rate (U+Th) (Gy/ka) [f]	Total dose rate (Gy/ka) [g]
GE16-1	57	24.5	212-250	0.46±0.02	1.02±0.05	0.02±0.01	0.03±0.01	1.53±0.08
GE16-1	57	24.5	90-125	0.46±0.02	1.09±0.05	0.02±0.01	0.03±0.01	1.61±0.08
GE16-2	38	8.1	212-250	0.43±0.02	0.73±0.04	0.02±0.01	0.03±0.01	1.22±0.06
GE16-3	72	24.2	212-250	0.25±0.02	0.46±0.02	0.02±0.01	0.03±0.01	0.75±0.04
GE16-4	97	28.2	250-300	0.21±0.01	0.79±0.04	0.02±0.01	0.03±0.01	1.05±0.06
GE16-5	155	23.2	212-250	0.33±0.02	0.75±0.04	0.02±0.01	0.03±0.01	1.13±0.06
GE16-6	32	15.3	212-250	0.64±0.02	1.19±0.06	0.02±0.01	0.03±0.01	1.89±0.09
GE16-6	32	24.5	90-125	0.64±0.02	1.27±0.06	0.02±0.01	0.03±0.01	1.97±0.09
GE16-7	76	21.3	212-250	0.54±0.02	1.23±0.06	0.02±0.01	0.03±0.01	1.82±0.09
GE16-7	76	21.3	90-125	0.54±0.02	1.31±0.07	0.02±0.01	0.03±0.01	1.91±0.10

[a] Water content, expressed as % of dry mass of sample and assigned a relative uncertainty of ± 20%.

[b] Radionuclide concentrations and specific activities have been converted to dose rates using the conversion factors given in Guérin et al. (2011) and Readhead (2002), making allowance for beta-dose attenuation (Mejdahl, 1979; Brennan, 2003).

[c] Gamma dose rates were calculated from *in situ* measurements made at each sample position with a NaI:Tl detector using the 'energy windows' method detailed in Arnold et al. (2012b).

[d] Beta dose rates were determined using a Risø GM-25-5 low-level beta counter (Bøtter-Jensen and Mejdahl, 1988), after making allowance for beta dose attenuation due to grain-size effects and HF etching (Brennan, 2003).

[e] Cosmic-ray dose rates were calculated following Prescott and Hutton (1994) and assigned a relative uncertainty of ± 10%.

[f] Assumed internal (alpha plus beta) dose rate for the quartz fractions are based on published ^{238}U and ^{232}Th measurements for etched quartz grains from a range of locations (e.g. Mejdahl, 1987; Bowler et al., 2003; Jacobs et al., 2006b; Pawley et al., 2008) and an alpha efficiency factor (a-value) of 0.04 ± 0.01 (Rees-Jones, 1995; Rees-Jones and Tite, 1997).

[g] Mean ± total uncertainty (68% confidence interval), calculated as the quadratic sum of the random and systematic uncertainties.

Table S1. Environmental dose rate values calculated for the quartz fractions of the Galería de las Estatuas samples.

Sample	Radionuclide specific activities (Bq/kg) [a, b]						Daughter: parent isotopic ratio		
	^{238}U	^{226}Ra	^{210}Pb	^{228}Ra	^{228}Th	^{40}K	^{226}Ra:^{238}U	^{210}Pb:^{226}Ra	^{228}Th:^{228}Ra
GE16-1	51.4 ± 6.6	46.2 ± 3.1	43.2 ± 4.9	40.5 ± 3.6	43.2 ± 3.2	342 ± 12	0.90 ± 0.13	0.94 ± 0.13	1.07 ± 0.13
GE16-2	19.5 ± 2.6	18.3 ± 1.3	18.8 ± 2.2	16.3 ± 1.5	16.4 ± 1.3	134 ± 5	0.94 ± 0.14	1.03 ± 0.14	1.00 ± 0.12
GE16-3	32.4 ± 4.1	22.9 ± 3.2	18.8 ± 2.2	14.2 ± 1.4	14.7± 1.2	123 ± 5	0.71 ± 0.13	0.82 ± 0.15	1.03 ± 0.13
GE16-4	62.3 ± 7.6	35.3 ± 8.2	26.6 ± 3.0	26.7 ± 2.4	27.8 ± 2.1	232 ± 8	0.57 ± 0.15	0.75 ± 0.19	1.04 ± 0.12
GE16-5	29.8 ± 3.8	24.1 ± 1.9	21.5 ± 2.5	31.4 ± 2.8	31.3 ± 2.3	271 ± 9	0.81 ± 0.12	0.89 ± 0.13	1.00 ± 0.12
GE16-6	37.1 ± 4.7	36.6 ± 2.5	36.1 ± 4.1	47.6 ± 4.1	47.9 ± 3.5	393 ± 13	0.99 ± 0.14	0.99 ± 0.13	1.00 ± 0.11
GE16-7	62.0 ± 7.8	46.3 ± 5.4	40.8 ± 4.7	46.4 ± 4.2	48.6 ± 3.7	372 ± 13	0.75 ± 0.13	0.88 ± 0.14	1.05 ± 0.12

[a] Measurements made on dried and powdered sediment sub-samples of ~120 g.
[b] Mean ± total uncertainty (68% confidence interval), calculated as the quadratic sum of the random and systematic uncertainties.

Table S2. High-resolution gamma spectrometry (HRGS) results for luminescence dating samples collected from Galería de las Estatuas. The specific activities of ^{238}U (determined from ^{235}U emissions after correcting for ^{226}Ra interference), ^{226}Ra (derived from ^{214}Pb and ^{214}Bi emissions), ^{210}Pb, ^{228}Ra (derived from ^{228}Ac emissions), ^{228}Th (derived from ^{212}Pb, ^{212}Bi and ^{208}Tl emissions) and ^{40}K were measured for each sediment sample, and used to calculate daughter-to-parent isotope ratios for ^{226}Ra:^{238}U, ^{210}Pb:^{226}Ra and ^{228}Th:^{228}Ra.

A			B		
Step	**Single-grain OSL**		**Step**	**Single-grain TT-OSL**	
1[a]	Give dose		1[a]	Give dose	
2 [b]	Stimulate with infrared diodes at 50ºC for 40 s (90% power)		2	Preheat to 260ºC for 10 s	
3	Preheat to 240ºC for 10 s		3	Stimulate with green laser at 125ºC for 2 s (90% power)	
4	Stimulate with green laser at 125ºC for 2 s (90% power)	OSL L_n or L_x	4	Preheat to 260ºC for 10 s	
5	Give test dose		5	Stimulate with green laser at 125ºC for 3 s (90% power)	TT-OSL L_n or L_x
6	Preheat to 160ºC for 10 s		6	Stimulate with blue LEDs at 280ºC for 400 s	
7	Stimulate with green laser at 125ºC for 2 s (90% power)	OSL T_n or T_x	7	Give test dose	
8	Return to 1		8	Preheat to 260ºC for 10 s	
			9	Stimulate with green laser at 125ºC for 2 s (90% power)	
			10	Preheat to 260ºC for 10 s	
			11	Stimulate with green laser at 125ºC for 3 s (90% power)	TT-OSL T_n or T_x
			12	Stimulate with blue LEDs at 290ºC for 400 s	
			13	Return to 1	

[a] Step omitted when measuring the natural signal (L_n).
[b] Step added only when measuring the OSL-IR depletion ratio described in Duller (2003).

Table S3. SAR protocols used in this study to obtain single-grain OSL (protocol A) and single-grain TT-OSL (protocol B) ages. L_n and L_x refer to the natural and regenerative-dose signal measurements, respectively. T_n and T_x refer to the test dose signals measured after the L_n and L_x signals, respectively.

Sample	Given dose (Gy)	accepted/ measured	Recycling ratio [a]	CAM D_e (Gy) [a]	OD (%) [a]
GE16-7	None (natural)	35 / 700	1.03 ± 0.05	161 ± 10	21 ± 8
GE16-7	148 ± 3	40 / 600	0.96 ± 0.04	327 ± 19	19 ± 7
		Measured D_e (after natural dose subtraction)		166 ± 22	
		Dose recovery ratio		**1.12 ± 0.14**	

[a] Mean ± total uncertainty (68% confidence interval), calculated as the quadratic sum of the random and systematic uncertainties.

Table S4. Single-grain TT-OSL dose recovery test results obtained for 90-125 μm quartz grains of sample GE16-7.

Sample	Grains measured (n)	Rejected grains (%)									Accepted grains (%)
		T_n signal <3xBG	Poor low dose recycling ratio	Poor high dose recycling ratio	IR depletion ratio	Recuperation >5%	Net T_n error >30%	L_n/T_n not intercepting DRC	Anomalous dose-response curve	Saturated	
GE16-1	1700	60	9	4	2	<1	11	1	3	5	5
GE16-1 (DRT)	800	60	7	6	4	0	11	0	4	3	5
GE16-2	1300	66	9	4	2	<1	10	<1	3	3	4
GE16-3	900	62	9	5	2	<1	10	<1	2	4	6
GE16-4	700	32	10	5	5	0	17	2	9	12	9
GE16-5	1500	58	8	3	4	<1	13	<1	3	5	7
GE16-6	1400	57	8	4	5	<1	12	<1	3	5	6
GE16-7	900	42	6	6	4	<1	15	2	6	9	9

Table S5. Single-grain OSL statistics showing proportion of rejected and accepted grains after applying the SAR rejection criteria. Data are also shown for the single-grain OSL dose recovery test (DRT) measurements made on sample GE16-1 (second row).

Sample	Grain size	Grains measured (n)	Rejected grains (%)									Accepted grains (%)
			T_n signal <3xBG	Poor low dose recycling ratio	IR depletion ratio	Recuperation >5%	Net T_n error >30%	L_n/T_n not intercepting DRC	Anomalous dose-response curve	Saturated	Slow decay	
GE16-1	90-125	1100	73	6	<1	<1	16	<1	1	<1	1	3
GE16-4	250-300	1400	81	5	<1	<1	12	<1	1	<1	<1	1
GE16-6	90-125	1400	70	6	<1	<1	17	<1	2	<1	1	3
GE16-7	90-125	700	60	9	<1	1	21	<1	3	<1	2	5

Table S6. Single-grain TT-OSL statistics showing proportion of rejected and accepted grains after applying the SAR rejection criteria.

Site	Region	Site type	Level	Sample	Age [a]	^{14}C cal. age (cal ka BP) [b]	Method	Reference
Prado Vargas	Cornejo, Burgos	Cave	4	Horse tooth	46.4 ka		AAR	Navazo et al. (2005)
Cueva Millan	Hortigüela, Burgos	Cave	1a 1b	Charcoal (GrN-11021) Charcoal (GrN-1161)	37.6 ± 0.7 ka 37.4 ± 0.6 ka	38.9–41.1 ka 38.9–40.9 ka	conv. ^{14}C (uncalibrated) conv. ^{14}C (uncalibrated)	Moure and García (1982) Moure and García (1982)
La Mina	Hortigüela, Burgos	Cave		Tooth (LEB-6012)	52.5 ka		AAR	Díez et al. (2008)
Valdegoba	Huérmeces, Burgos	Cave	7 5	Capping stalagmitic flowstone Bone (OxA-21970)	<73.2 ± 5 ka 48.4 ± 3.3 ka	 >48 ka	U-series AMS ^{14}C ultrafiltration (uncalibrated)	Quam et al. (2001) Dalen et al. (2012)
Hotel California	Atapuerca, Burgos	Open-air	V V II I	Sedimentary quartz grains (HC10-1) Sedimentary quartz grains (HC10-4) Sedimentary quartz grains (HC10-2) Sedimentary quartz grains (HC10-3)	48.2 ± 3.3 ka 48.2 ± 3.9 ka 57.6 ± 5.7 ka 71.0 ± 5.6 ka		Single-grain OSL Single-grain OSL Single-grain OSL Single-grain OSL	Arnold et al. (2013) Arnold et al. (2013) Arnold et al. (2013) Arnold et al. (2013)
Hundidero	Atapuerca, Burgos	Open-air	2 2 3 4	Sedimentary quartz grains Sedimentary quartz grains Sedimentary quartz grains Sedimentary quartz grains	30.2 ± 3.6 ka 58.8 ± 4.9 ka 56.2 ± 4.4 ka 70.6 ± 11 ka		OSL TL OSL TL	Navazo et al. (2011) Navazo et al. (2011) Navazo et al. (2011) Navazo et al. (2011)
Galería de las Estatuas	Atapuerca, Burgos	Cave	Base GE-I, LU1 GE-I, LU1 GE-I, LU1 GE-I, LU2 GE-I, LU2 GE-I, LU2 GE-I, LU2 GE-I, LU3 GE-I, LU3 GE-I, LU3 GE-I, LU4 GE-II, LU1b GE-II, LU1 GE-II, LU2 GE-II, LU2	Capping flowstone Bone (Beta - 247621) Bone (OxA-21523) Sedimentary quartz grains (GE16-2) Bone (Beta - 247672) Bone (OxA-21524) Sedimentary quartz grains (GE16-1) Sedimentary quartz grains (GE16-3) Bone (Beta - 247628) Bone (OxA-21525) Sedimentary quartz grains (GE16-4) Sedimentary quartz grains (GE16-5) Bone (OxA-24563) Sedimentary quartz grains (GE16-6) Bone (OxA-24564) Sedimentary quartz grains (GE16-6)	14. 2 ± 0.3 ka >45 ka 43.5 ± 1.8 ka 80 ± 5 ka >45 ka >45.6 ka 80 ± 5 ka 113 ± 8 ka >45 ka 44.0 ± 1.9 ka 107 ± 8 ka 111 ± 7 ka 44.2 ± 2.0 ka 69 ± 4 ka >46.3 ka 80 ± 5 ka	 44.7–>48 ka 43.0–>48 ka 43.2–>48 ka 	U-series AMS ^{14}C standard AMS ^{14}C ultrafiltration Single-grain OSL AMS ^{14}C standard AMS ^{14}C ultrafiltration Single-grain OSL Single-grain OSL AMS ^{14}C standard AMS ^{14}C ultrafiltration Single-grain OSL Single-grain OSL AMS ^{14}C ultrafiltration Single-grain OSL AMS ^{14}C ultrafiltration Single-grain OSL	Martinez-Pillado et al. (2014) Arsuaga et al. (2017) Arsuaga et al. (2017) This study Arsuaga et al. (2017) Arsuaga et al. (2017) This study This study Arsuaga et al. (2017) Arsuaga et al. (2017) This study This study Arsuaga et al. (2017) This study Arsuaga et al. (2017) This study
La Ermita	Hortigüela, Burgos	Cave	 5a	Capping flowstone Capping flowstone Charcoal (OxA-4603)	95 ± 6 ka 102 ± 4 ka 31.1 ± 0.6 ka	 32.1–34.2 ka	U-series U-series AMS ^{14}C (uncalibrated)	Sánchez Yustos and Diez Martín (2016) Sánchez Yustos and Diez Martín (2016) Díez et al. (2008)

			5a 5a	Tooth Tooth	114 ± 42 ka 129 ± 39 ka		AAR AAR	Díez et al. (2008) Díez et al. (2008)
San Quirce	San Quirce, Palencia	Open-air	Bed 6	Sedimentary quartz grains (SQ 1; C-L 3066)	73 ± 10 ka		Single-grain OSL	Terradillos-Bernal et al. (2017)
Cueva Corazon	Mave, Palencia	Cave	2 2	Burned lithic (MAD-4712BIN) Burned lithic (MAD-4715BIN)	97 ± 8 ka 96 ± 7 ka		TL TL	Diez Martín et al. (2011) Diez Martín et al. (2011)
El Castillo	Puente Viesgo, Cantabria	Cave	23c	Travertine	89 ± 10 ka		U-series	Bischoff et al. (1992)
Cueva del Camino	Pinilla del Valle, Madrid	Cave	South sector 8 5 3 (fluvial)	Sedimentary quartz grains Sedimentary quartz grains Sedimentary quartz grains Sedimentary quartz grains	74.5 ± 6.3 ka 91.6 ± 8.1 ka 90.9 ± 7.8 ka 140.4 ± 11.3 ka		TL TL TL TL	Arsuaga et al. (2012) Arsuaga et al. (2012) Arsuaga et al. (2012) Arsuaga et al. (2012)
Las Callejuelas	Monteagudo del Castillo, Teruel		91 cm 94 cm 164 cm Uncertain Uncertain	(LEB 8533) (LEB 8529) (LEB 8532) (LEB 8530) (LEB 8531)	116 ka 122 ka 135 ka 190 ka 252 ka		AAR AAR AAR AAR AAR	Domingo et al. (2017) Domingo et al. (2017) Domingo et al. (2017) Domingo et al. (2017) Domingo et al. (2017)

[a] Age uncertainties presented at 1σ.
[b] Calibrated age presented at 95.4% probability range
AAR = amino acid racemisation; AMS ^{14}C = accelerator mass spectrometry; conv. ^{14}C = conventional ^{14}C; ESR = electron spin resonance; OSL = optically stimulated luminescence; TL = thermoluminescence. ^{14}C dates were calibrated using OxCal 4.2 (Bronk Ramsey and Lee, 2013) and the Intal13 atmospheric curve (Reimer et al., 2013).

Table S7. Regional dating context of Middle Palaeolithic sites across northern Spain mentioned in the text.